FORMING PROPERTIES OF STRETCH BROKEN CARBON FIBER FOR AIRCRAFT STRUCTURES

by

Dalton Bradley Nold

A thesis submitted in partial fulfillment
of the requirements for the degree

of

Master of Science

in

Mechanical Engineering

MONTANA STATE UNIVERSITY
Bozeman, Montana

June 2023

ACKNOWLEDGEMENTS

I would like to express my sincere gratitude and appreciation to my parents Brad and Jennifer Nold, for their support and encouragement throughout my life. Their unwavering affection and belief in me have been the foundation of my success, and I couldn't have accomplished so much without their constant support.

I am pleased to express my sincere appreciation to my brother Seth Nold, whose generous financial support enabled me to pursue my academic endeavors without the added burden of worrying about living expenses. His kindness and support have been instrumental in my success, and I am forever grateful for his invaluable contribution to my personal and professional growth.

A heartfelt expression of gratitude goes to my esteemed advisor and department head, Dr. Dilpreet Bajwa, whose guidance and support propelled me to perform at the highest level throughout my degree.

Finally, I would like to express a special thanks to the entire Stretch Broken Carbon Fiber Research Group at Montana State University. This includes esteemed faculty, skilled professionals, and talented graduate and undergraduate students. Their valuable guidance, support, and collaboration have made my experience working with them an absolute pleasure.

This work was supported by The US Department of the Army (Contact number: W911W6-18-C-0050). The views and conclusions contained in this document are those of the authors and should not be interpreted as necessarily representing the official policies, either expressed or implied, of the Government.

TABLE OF CONTENTS

TABLE OF CONTENTS CONTINUED

LIST OF TABLES

Table Page

LIST OF FIGURES

Figure Page

LIST OF FIGURES CONTINUED

Figure Page

LIST OF FIGURES CONTINUED

Figure Page

LIST OF FIGURES CONTINUED

Figure Page

ABSTRACT

Continuous carbon fiber is known to be a superior material for its strength, stiffness, and high strength-to-weight ratio and is often incorporated in aerospace composites. A challenge, however, is that it's not versatile in forming deep drawn geometries, which require convoluted manufacturing techniques resulting in expensive components. To overcome this, a type of carbon fiber with a random discontinuous fiber alignment called stretch broken carbon fiber (SBCF) is proposed. SBCF has potential to form parts with complex geometries with comparable or better mechanical properties to that of continuous carbon fiber. Montana State University (MSU) developed its own version of SBCF manufacturing processes, and research is being conducted to understand how SBCF prepreg tows react to stretch drawing at elevated temperatures using aerospace-grade epoxy resin systems. Currently, several new methods have been proposed to rapidly test these materials. This research revealed that SBCF forms with greater ease than continuous carbon fiber and is expected to substantially reduce manufacturing times for aircraft structures. To comprehend the material's behavior, simple tensile tests were coursed to understand how gauge length and temperature affected the peak loads when compared to continuous carbon fiber. It was discovered that on average, SBCF experienced stresses that were ten times less than continuous fibers.

Additional tensile tests were conducted at elevated temperature to determine the true stress versus true strain. These tests are particularly important because they represent the material's most accurate mechanical properties. The results led to the discovery that SBCF experienced strain softening behavior.

Furthermore, a series of forming tests using a novel "forming fixture" revealed that increasing the gap lowered the peak forming loads while the plunger geometry had little to no effect on peak forces at both room and elevated temperatures.

CAPTER ONE

LITERATURE REVIEW

Composite Materials

Composites are unique materials formed by combining two or more distinct components, resulting in a novel material that exhibits improved characteristics [1]. composite materials have gained a wide variety of popularity in various engineering applications due to their exceptional strength and stiffness while remaining extremely lightweight [1, 8-13]. This literature review will explore applications, manufacturing techniques, environmental impacts, and advancements in composite materials research.

Applications of Composite Materials

Composite materials have many uses in industrial subdivisions, such as aerospace, automotive, marine, and civil construction. In the aerospace industry, composites are primarily used for their high strength-to-weight ratio and low thermal expansion [15, 16, 21]. They have been used for many primary components, such as aircraft structures, landing gears, and engine mechanisms [23]. Previous studies have shown the effectiveness of composites' high mass-specific energy absorption capabilities under crash analysis from a finite element model. The energy absorption capabilities were essential due to the difficulty of simulating composites for heavier ductile metals [22].

In the automotive industry, composite materials have made high performance car bodies, bumpers, and fenders due to their lightweight and impact absorption, saving millions of lives.

Additionally, composite materials are used in the construction industry for fabricating bridges, high-rise buildings, and many other infrastructural structures and projects. Moreover, composite materials have applications in sports equipment, medical devices, and electronics.

Manufacturing Techniques

As mentioned previously, manufacturing a composite material involves the combination of two or more materials with different properties. Several techniques are used for manufacturing composite materials: hand layup, filament winding, pultrusion, injection molding, and 3D printing. Hand layups are the most common and straightforward technique used in the industry, involving the layering of composite materials by hand. The downside is that it takes a long time, as some composite layups can have up to 100 or more layers, increasing manufacturing time and costs. Filament winding is used for manufacturing structures such as pipes, tanks, and pressure vessels used in aerospace, marine, and ordinance applications [24]. Pultrusion involves the continuous production of composite materials with a fixed cross-section. A perfect example is how continuous polymer-reinforced fibers are produced. Injection molding is a relatively new technique that enables the production of composite parts with intricate geometries. Typically used in manufacturing thermoplastics, a high-value composite material is a cellulose nanocomposite. These crystals are injection molded with high density polyethylene matrix at low enough temperatures to keep the bio-based cellulose nanocrystals from burning. These materials have improved mechanical properties due to the versatility of the cellulose found in nature [26].

Environmental Impacts

The manufacturing of composite materials can result in environmental impacts and can also be challenging to recycle due to their heterogeneous hybrid structure. However, composite materials can contribute to environmental sustainability by reducing the weight of structures and vehicles, resulting in lower fuel consumption and emissions [25]. Moreover, developing newer composite materials made from renewable resources, such as bio-based and recycled materials, can further enhance the environmental sustainability of composites. An additional means by which composites may exert a more positive impact on the environment is through their heightened wear resistance, thereby obviating the need for replacement.

Advancements in Composite Materials

Developing new composite materials is a continuous process, and researchers are exploring new combinations of materials to create novel composites with enhanced properties. Recent advancements in composite materials research have led to the development of nanocomposites, polymer matrix composites, metal matrix composites, and ceramic matrix composites. Nanocomposites have gained attention due to their exceptional mechanical, thermal, and electrical properties. Polymer matrix composites are used in various applications due to their outstanding durability and low weight. Metal matrix composites are widely used in aerospace and automotive industries due to their high strengths and stiffnesses and their wear resistance, making them last much longer. Ceramic matrix composites are known for their superb thermal and mechanical properties, making them suitable for high-temperature applications.

Conclusion

In summary, composite materials have become essential to many industries due to their extraordinary properties. The use of composite materials is expected to increase as the demand for lightweight and durable materials grows in the engineering paradigm. The manufacturing techniques for composite materials continue to advance, developing new and innovative products. The environmental impacts of composite materials must also be considered, and efforts must be made to develop sustainable composites with reduced environmental footprints.

CHAPTER TWO

INTRODUCTION TO STRETCH BROKEN CARBON FIBER

Rationale

The adoption of carbon fiber-based composite materials has contributed to the aerospace industry since the discovery of carbon fiber in 1963 at the Royal Aircraft Establishment in Farnborough, UK [1]. A superior form of carbon fiber is produced from processing polyacrylonitrile (PAN) based polymers, which are widely used in high-value applications in the aerospace industry. PAN-based carbon fiber composites can generate more than 50% of an aircraft's structural mass, which relates to researching and innovating this material even further [1]. Composites comprising of PAN-based carbon fibers demonstrate superior characteristics in an aircraft, including reduced weight, heightened fuel efficiency, and enhanced resistance to corrosion. Furthermore, these composites are comparable to titanium in strength and stiffness, despite the latter being a considerably denser material. [2,3]. Figure 2.1 depicts a detailed schematic showcasing the fundamental principle of composite formation, where fiber and matrix interact to create a new material with superior properties. Additional layers, or "lamina," are introduced to reinforce areas of heightened stress, thereby enhancing the strength of the resultant stacking sequence, or "laminate."

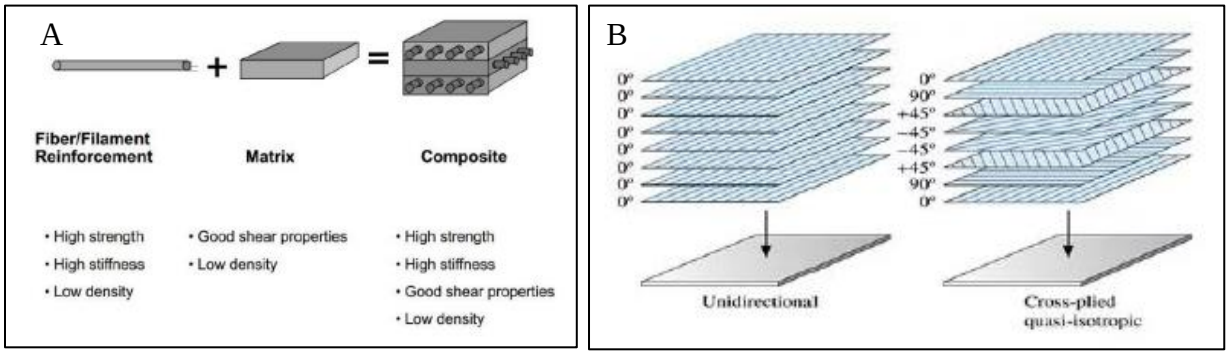

Figure 2.1: (A) Carbon fiber composite composition [18] (B) Laminate orientation design [14]

The design of a carbon fiber reinforced polymer (CFRP) incorporates a strategic arrangement of fibers that corresponds with the location of the load application. Fibers can be organized to impart equivalent stiffnesses and strengths regardless of the direction of the load application, a process referred to as "isotropy," to achieve homogeneity across the laminate. This laminate is subsequently overlaid onto a geometric structure and subjected to molding and curing procedures that conventionally entail pressure and heat. Below is an accompanying diagram that illustrates this concept.

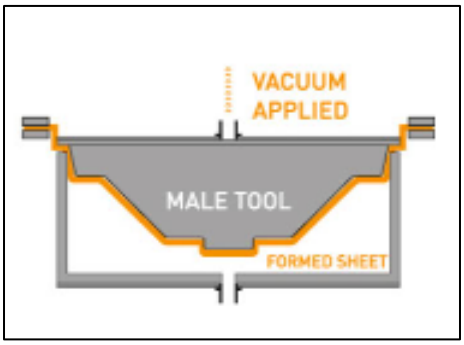

Figure 2.2: Example of a traditional forming process

One of the prevailing challenges associated with integrating carbon fiber composites into primary aircraft structures is the limited adaptability of the manufacturing process to create parts featuring intricate geometries characterized by filleted 90° corners and deep-drawn shapes. In the

context of beam bending, maximizing the moment of inertia is essential to mitigate the effects of bending stress and ensure the structural integrity of the mechanical subsystem. The beam's cross-sectional area determines the moment of inertia (I). In part, optimizing the geometry of the beam allows for the maximization of the moment of inertia. The diagrams below illustrate several conventional beam designs utilized in structures with complex geometries and demonstrate how the moment of inertia can be optimized to minimize bending stress.

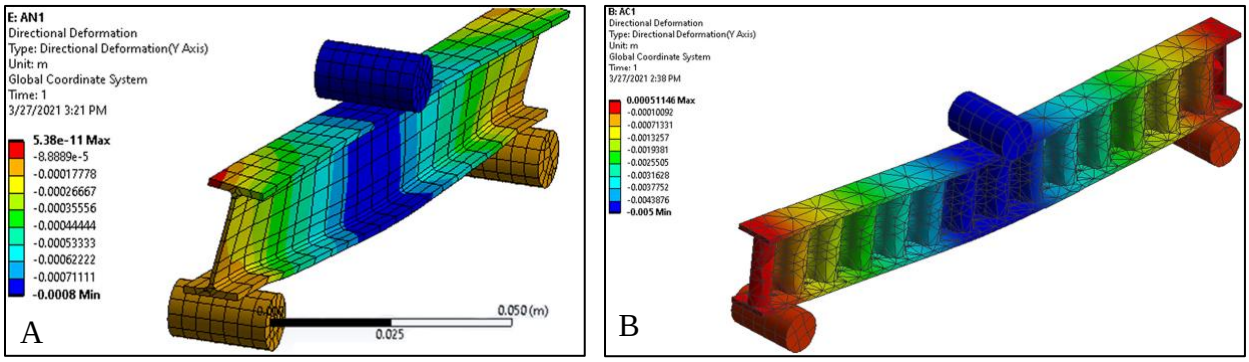

Figure 2.3: (A) Finite element analysis of a traditional I beam under 3-point bending (B) Finite element analysis of a sinusoidal I beam under 3-point bending [17]

I Beam Area Moment of Inertia Formula

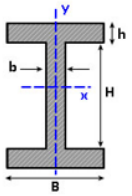

Parameter	Equation
Area moment of inertia	$I_{xx} = \frac{H^3 b}{12} + 2\left[\frac{h^3 B}{12} + hB\frac{(H+h)^2}{4}\right]$
Area moment of inertia	$I_{yy} = \frac{H^3 b}{12} + 2\left[\frac{h^3 B}{12}\right]$

Figure 2.4: Example illustrating how to calculate the moment of inertia of a simple I-beam.
Equation 2.1: Bending stress equation for beams

Bending Stress: $\boldsymbol{\sigma = \frac{My}{I_{xx}}}$

To fabricate CFRP components, consolidation of carbon fibers within an uncured, resin-impregnated sheet commonly referred to as prepreg is necessary [2]. The resulting part can then be subjected to elevated pressure and temperature, depending on the curing thermoset matrix. However, in cases where the mold geometry is highly intricate, such as deep-drawn shapes, continuous carbon fiber prepreg formation is challenging due to the material's low strain-to-failure ratio (~2%). Figure 2.5 depicts the respective manufacturing defects associated with this context.

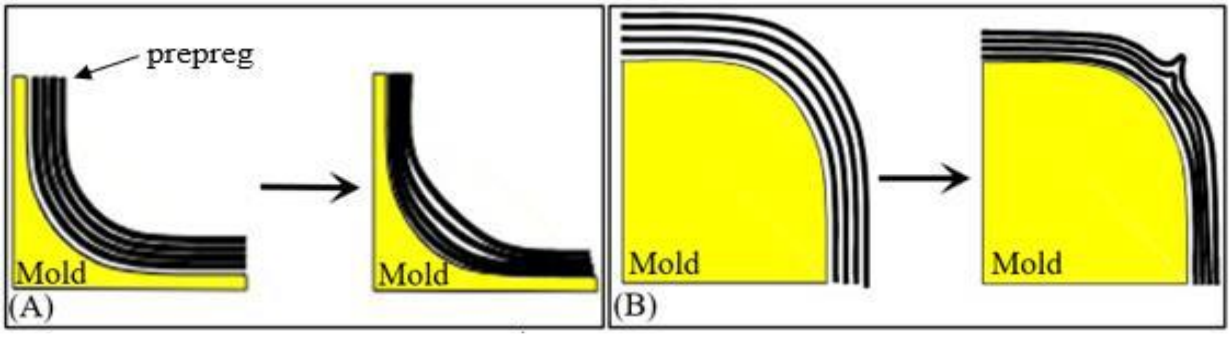

Figure 2.5: (A) Deep draw ply delamination (B) Wrinkling defect [16]

It is necessary to subject the carbon fiber prepreg to a process of pseudo-plastic deformation in the fiber direction during the forming process. The pseudo-plastic deformation would facilitate its accommodation to the mold at a reduced forming pressure. It would maintain the same strength and stiffness levels achieved using continuous carbon fiber once a finalized part is cured. This objective can be achieved by converting a continuous fiber prepreg into a discontinuous fiber prepreg, whereby the broken fibers are randomly dispersed throughout the material’s length, width, and thickness while preserving the uniformity of fiber alignment. Such

an approach enables the fibers to move against each other in the fiber direction while maintaining the viscosity of the matrix to facilitate consolidation and molding of the prepreg. The resulting carbon fiber variant is called stretch-broken carbon fiber (SBCF) prepreg, which can retain between 95-100% of the strength and stiffness of continuous carbon fiber once the part is cured [4, 5, 8-12]. Figure 2.6 below serves as empirical evidence of this assertion.

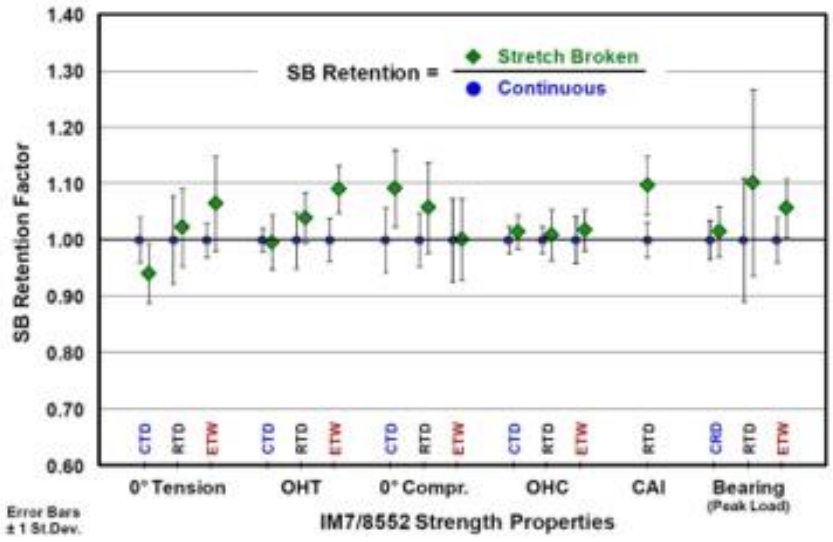

Figure 2.6: Mechanical retention comparison of continuous and SBCF materials [4]

Direct to Prepreg Manufacturing

Montana State University has devised multiple proprietary technologies to manufacture SBCF. As illustrated in Figure 2.7, two distinct equipment lines have been developed to facilitate the stretch-breaking process. The present study focused on the material produced through a modified version of the first equipment line (depicted as 'A' in Figure 2.7). This technique involved the integration of stretch breaking with a resin film, referred to as 'Direct to Prepreg' or DTP [4, 6].

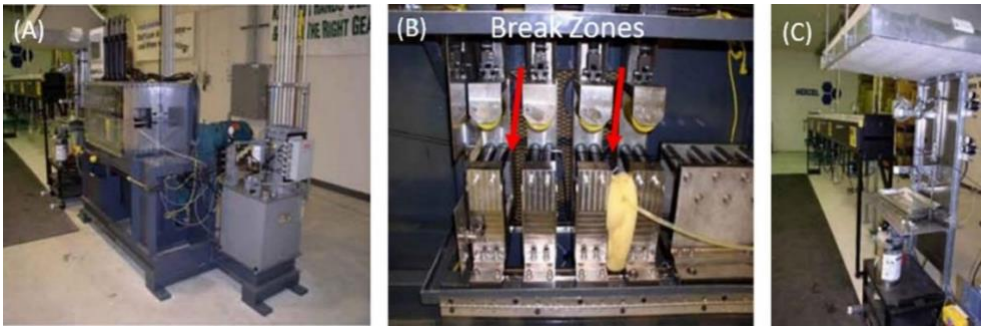

Figure 2.7: (A) Hexcel stretch breaking machine (B) Breaking zones on stretch breaking machine (C) Sizing application station on stretch breaking machine [2]

This process takes ten spools of continuous carbon fiber tows and stretch breaks them simultaneously. Figure 2.8 depicts a schematic representation of the stretch-breaking process where rollers apply a high inward nip force of up to 0.5 KN. The breakage occurs because both sets of rollers move at differential speeds ($\omega_1 < \omega_2$), randomly breaking the fibers in tension at their natural flaws.

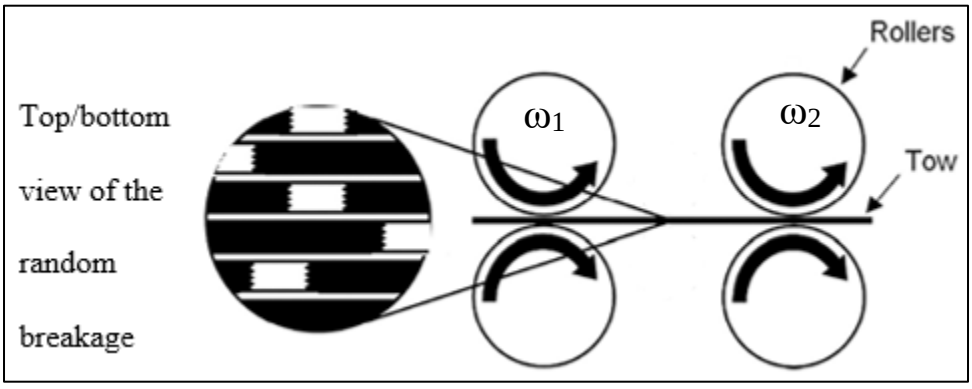

Figure 2.8: Side view schematic of stretch breaking process that breaks the fibers at random locations along the length and width of the tow [2, 16]

An additional schematic of the stochastic breakpoints is presented in conjunction with a Field-Emission Scanning Electron Microscopy (FE-SEM) image in Figure 2.9 B.

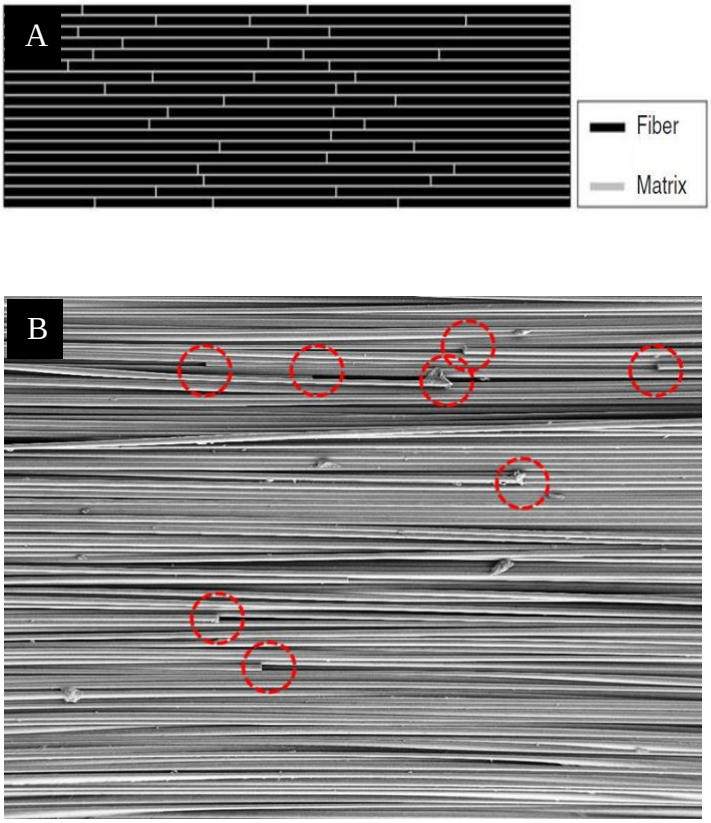

Figure 2.9: (A) Schematic of a stretch broken carbon fiber material (B) FE-SEM of a stretch broken carbon fiber material showing break locations [12]

Immediately following the process of fiber breakage, a resin film, as illustrated in Figure 2.10, is applied to the ribbon. The ribbon is then subjected to a secondary operation called belt compaction, depicted in Figure 2.11 A, in which it is compacted and further impregnated through high heat and pressure.

Figure 2.10: Resin film of uniform thickness to be applied to the 10 tow wide stretch broken ribbon

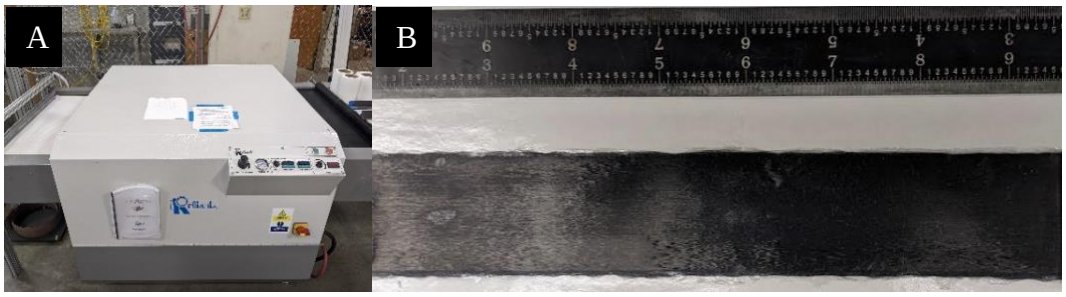

Figure 2.11: (A) Prepreg fusing compaction machine (B) 10 tow ribbon of MSU DTP

Bobcat Machine to Generate Single-Tow SBCF

The second method MSU used to produce SBCF was a method that broke the fibers in a similar way to the DTP. Notwithstanding, the product constituted a solitary tow wound onto a spool for distribution and solely maintained through a polymer sizing agent, lacking impregnation with the resin. The sizing application is meant to hold the fibers together for transportation and is further discussed in the next chapter. This process is illustrated below in Figure 2.12.

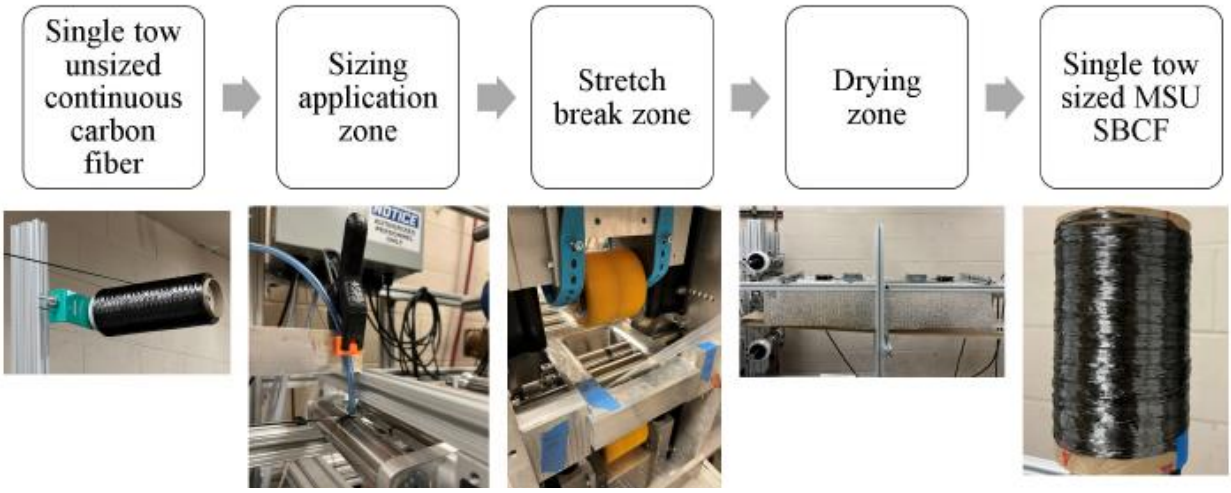

Figure 2.12: Flow diagram of single tow MSU SBCF production on the Bobcat machine [15]

DTP is an elegant way to make unidirectional prepreg tape but is currently limited in width by the available equipment. The difference between a single SBCF tow is that it is needed for prepregging on conventional industry equipment, conversion to woven fabric, and other formats such as braids and stitched multiaxial layups. It also requires a prepregger to invest in specialized stretch-breaking equipment. While this may happen at some point, the initial requirement from prepreggers will likely be for single tow spools to run on existing equipment.

Thesis Objectives

Prior research conducted by Hexcel Corporation had established an essential correlation between a smaller fiber break length and formability due to the fiber's ability to move with the matrix at shorter gauge lengths [1, 15]. The initial average break length was approximately 10 cm; however, a NAVAIR-funded program in 2006 was able to lower it to 5 cm [6]. With recent advances at Montana State University, stretch-broken carbon fiber prepreg had achieved an average break length of 3 cm. At the time of this publication, the present study achieved the

industry's minimal mean fiber length when examining fibers that experienced tensile failure at their inherent flaws, in contrast to fibers that underwent fragmentation through a chopping process [8-13]. The existing program's primary aim was to assess the forming properties of the prepreg, particularly for peak load versus displacement. These evaluations offered more comprehensive insights into the material's behavior and helped to understand how the material behaved throughout the forming process. To this end, the first two objectives were to test the SBCF in simple tension in two distinct ways. The first method involved testing the SBCF-sized tows at various gauge lengths and temperatures while comparing them to continuous carbon fiber behavior. This experiment used different nozzle heads from a heat distributor to apply convectional heat along the entire sample length. Infrared imaging was utilized to track the temperature of the tow samples to ensure that they maintained their elevated temperature for the entire test duration.

Once tensile data without the inclusion of resin impregnation was compared between continuous and stretch broken fibers, the second tensile test was performed to investigate the elastic modulus of stretch broken fibers with resin impregnation. Specifically, this test evaluated the single tow prepreg at the resin’s desired debulking temperatures to determine its true stress versus true strain. As the tensile test characterizes a material's most accurate representation of its mechanical attributes for integrity and safety, this data and experiment design was essential to quantify later for simulation for forming purposes alone.

After the results to characterize the properties of the stretch broken carbon fiber prepreg in its most accurate representation in unidirectional tension, the third objective was to develop a novel forming fixture to understand the impact of various geometric variables on the forming characteristics of SBCF [14, 21]. The forming fixture needed to be versatile both geometrically

and physically, capable of simulating different tool shapes and temperatures related to the forming process. Carbon fiber prepreg was then tested in the fixture to obtain load versus displacement data, allowing the investigation of load factors under various geometrical conditions of discontinuous CFRPs to begin stretching. This innovative approach provided insights into the material's behavior during the forming process and offered a glimpse into the future of advanced manufacturing techniques for high-performance composites.

CHAPTER THREE

THE INFLUENCE OF GAUGE LENGTH AND TEMPERATURE ON CONTINUOUS AND STRETCH BROKEN CARBON FIBER TOWS

Introduction

This chapter outlines the experimental investigations conducted to analyze the impact of gauge length and temperature on the tensile strength of MSU SBCF and conventional continuous carbon fiber tows. Prior research had reported substantial differences in the peak loading forces of continuous carbon fiber and SBCF generated by Hexcel Corporation [2]. It is common in industry to obtain stock material where a single tow of fibers are wound onto a spool and held together by a small polymer coating known as sizing [10, 15]. The sizing would act as a bonding agent between the fibers, making handling them much more manageable. Further down the manufacturing process, the resin would act as a solvent towards the sizing and replace it during its curing procedure. An FE-SEM cross-sectional image illustrates the bond between fiber and sizing in Figure 3.1.

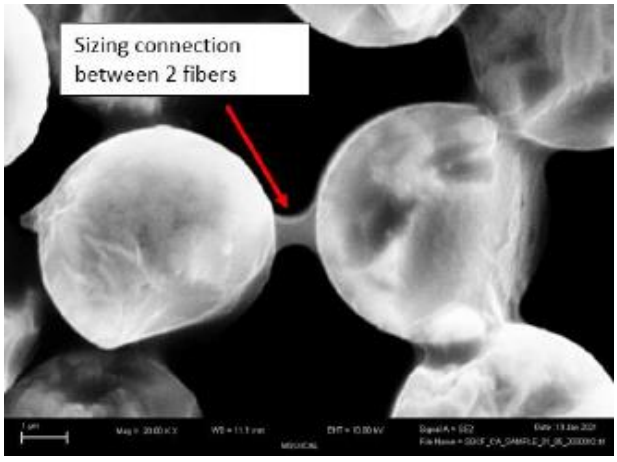

Figure 3.1: FE-SEM microscopy image of sizing bridge between carbon fiber filaments [21]

The spooled single-tow material is easily transported to a composite manufacturing center to make prepreg sheets, cylindrical tubing, or any part configuration the company can facilitate. This study aimed to compare the tensile stress thresholds of single-tow MSU SBCF with industry-produced continuous carbon fiber to draw scientific conclusions.

Materials

This experiment began with a spool of 12k IM7 fibers, which underwent one of two secondary operations in The Bobcat Machine. The first operation involved preparing the continuous material by applying a Michelman sizing and subsequently drying the tow to achieve a sizing weight percent of 1.86%. The other operation had the Michelman applied and then was stretch broken before allowing the sizing to dry. These different operations created two types of material that could then be easily transported for testing and their properties are tabulated in Table 3.1 below. The filament count and cross-sectional area of tows was calculated based on the fiber count, single fiber areal weight, and fiber diameter as described in the Hexcel Corporation technical data sheet [20].

Table 3.1: Material Properties of IM7-M and SBCF

	IM7-M	SBCF
Fiber Weight [g/m]	0.446	0.361
Fiber Count	12000	9716
Weight Per Fiber [g/m]	3.72×10^{-5}	3.72×10^{-5}
Filament Diameter [mm]	0.0052	0.0052
Filament Area (mm^2)	2.12×10^{-5}	2.12×10^{-5}
Cross-sectional area [mm^2]	0.25	0.206

Test Methodology

To prepare the continuous and discontinuous samples for testing, cardboard tabs were glued on each end with a fast-setting ethyl cyanoacrylate glue at gauge lengths of 6.35, 12.7, 25.4, 50.8, 76.2, 101.6, and 127 mm. Figure 3.2 illustrates the preparation method employed for each sample, which facilitated the secure gripping of the clamps and prevented slippage during the application of tensile force. A total of five samples were tested at each length. The two temperatures selected for testing were 20 °C (RT) and 100 °C (HT), consistent with previous work [2]. The widths of the test samples were 6.3 mm.

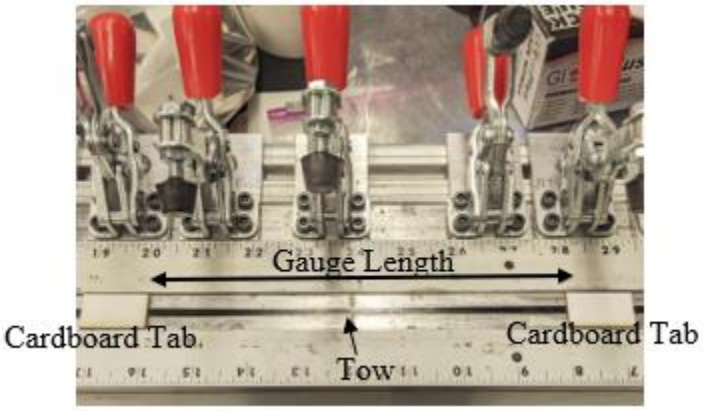

Figure 3.2: Single tow sample preparation

The peak stresses were determined from the load versus displacement data gathered from the tensile experiment. The samples were tested on a Mark 10 ESM 303 universal testing machine (Mark-10, Copiague, NY, USA) at a constant rate of 6.3 mm/min. A heat gun equipped with different nozzles was used to achieve uniform elevated temperature along the length of the sample and is shown in Figure 3.3. To ensure heat was being applied across the entire gauge length the nozzles had to be adjusted according to the gauge length of the test samples. As the sample gauge length continued to increase, a customized heat enclosure was integrated, and a schematic is shown

in figure 3.4. A Fluke thermal imager (Fluke Corporation, Everette WA, USA) was used to provide a real-time temperature reading during the test. An example of a recorded thermal image is shown in Figure 3.5.

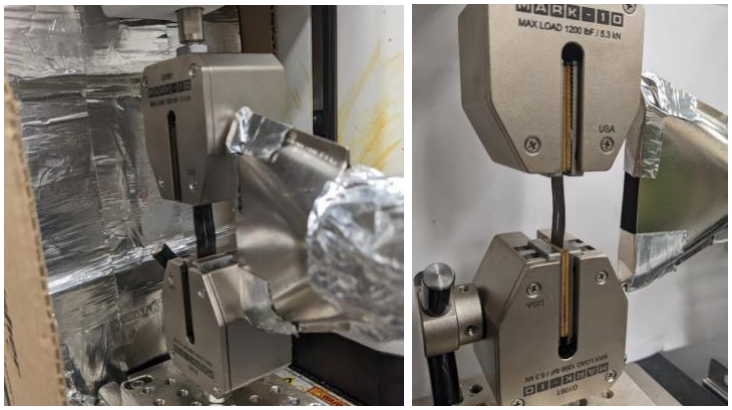

Figure 3.3: Heat gun equipped with different nozzles used for elevated temperature testing

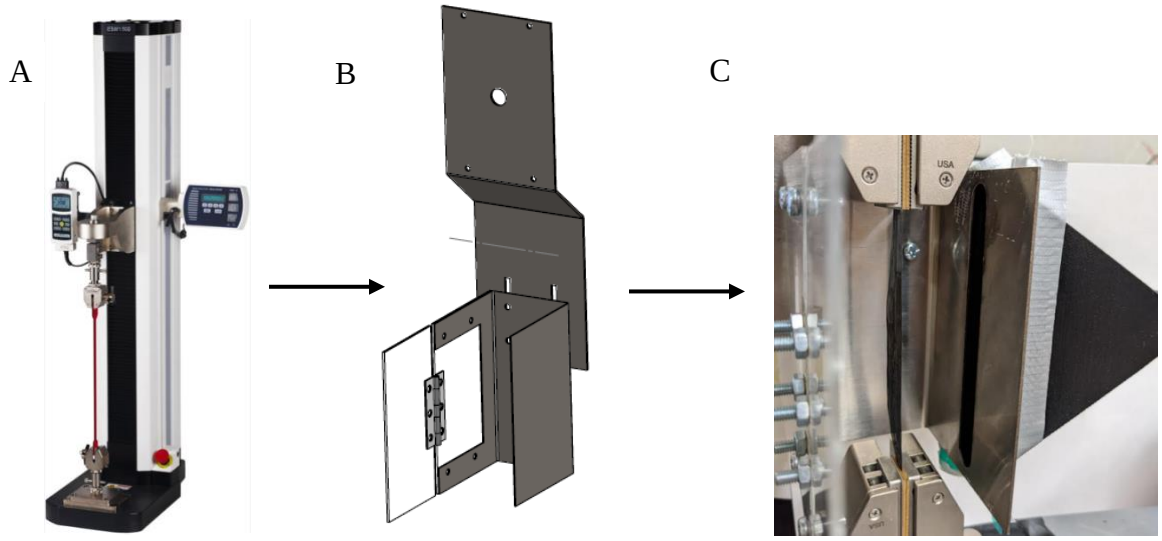

Figure 3.4: (A) Mark 10 ESM 303 (B) Heat enclosure design (C) Diffused heat onto test sample

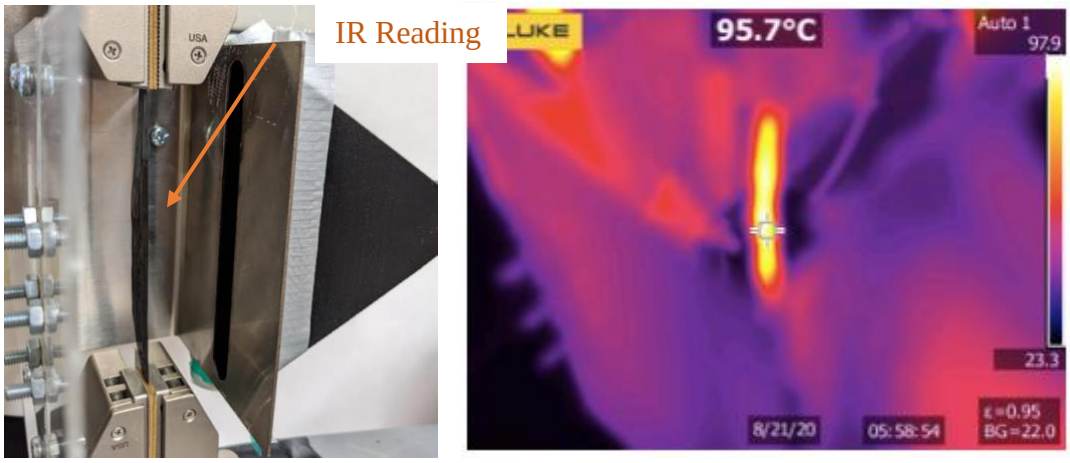

Figure 3.5: Fluke thermal imager analysis for real time temperature reading and displays uniform heating

As previously mentioned, each gauge length consisted of testing five samples that were averaged and plotted into several different charts. These charts display the average load versus displacement data followed by boxplots of stress versus gauge length. The final graph averages each of the five samples into a single data point for each of the gauge lengths accompanied by a curve fit line. This graph compares results from previous work.

Results and Discussion

The graphical representations of load-displacement relationships for continuous and MSU SBCF at varying temperatures are presented in Figure 3.6 A-D. The continuous carbon fiber tows failed within the load range of 550-800 N, whereas the MSU SBCF failed within the load range of 2-250 N. The observed augmentation in peak load for the shorter gauge lengths was anticipated, given the decreased number of intrinsic flaws in the fibers. In the case of the SBCF material, the fibers were interconnected through the connection of the sizing, which notably decreased the peak forces upon deformation due to the shear forces between the sizing and the fibers.

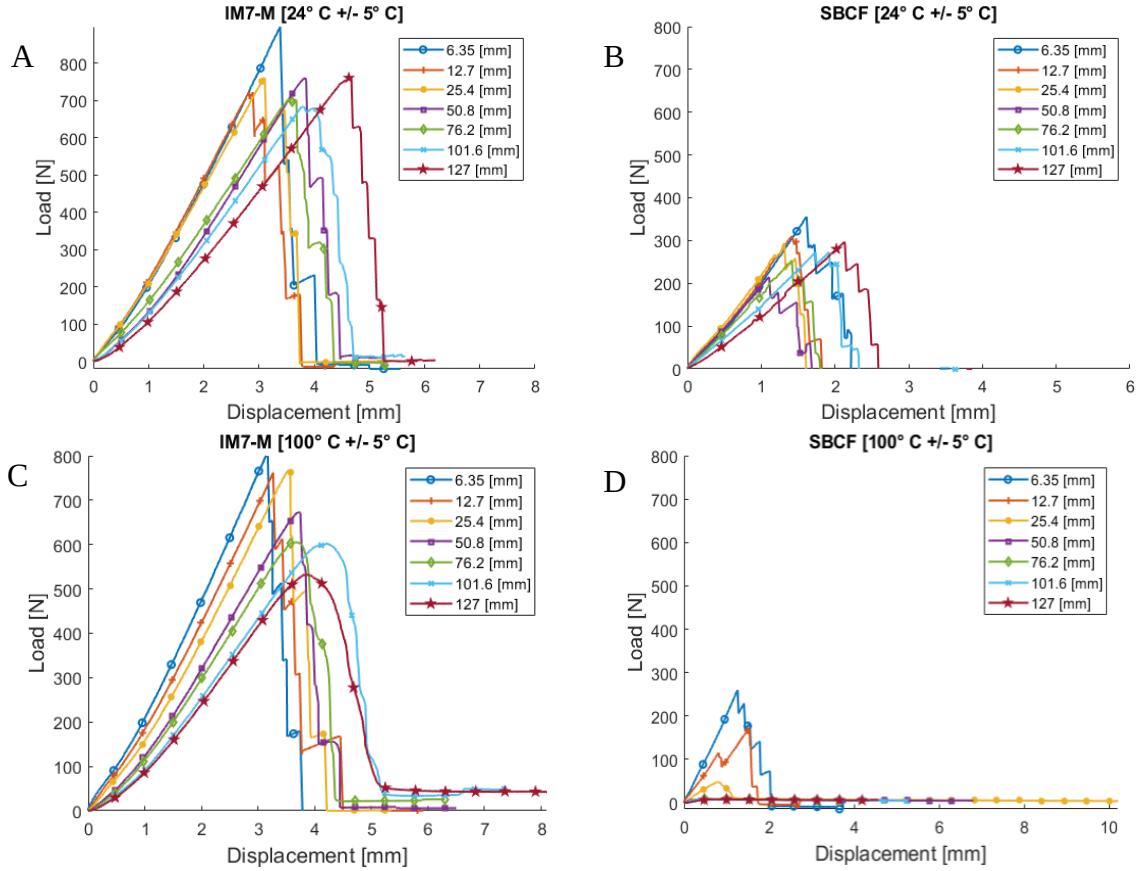

Figure 3.6: (A) Room temperature load vs. displacement curves of continuous and (B) MSU SBCF (C) Elevated temperature load vs. displacement curves of continuous and (D) MSU SBCF

The boxplots depicted in Figure 3.7 A-D provide an insight into the distribution of maximum stress failure across each of the five samples tested in this study. The comparative analysis of peak stresses in response to gauge length increments for continuous and discontinuous fibers under the varying temperature conditions can be observed in these figures. Figures 3.7 A and C illustrate the comparisons of peak stresses at ambient and elevated temperatures between the continuous fiber tows. There was no distinct difference in the data resulting in the conclusion that temperatures between 20 °C– 100 °C did not affect the tensile strength of continuous carbon fiber tows. Notably, a persistent decline in stress was observed as the gauge length approached the 3 cm mean fiber length of MSU SBCF, indicating favorable behavior. Moreover, this phenomenon

translated into lower forming stresses with an increase in gauge length, which is a desirable characteristic in forming fiber composites.

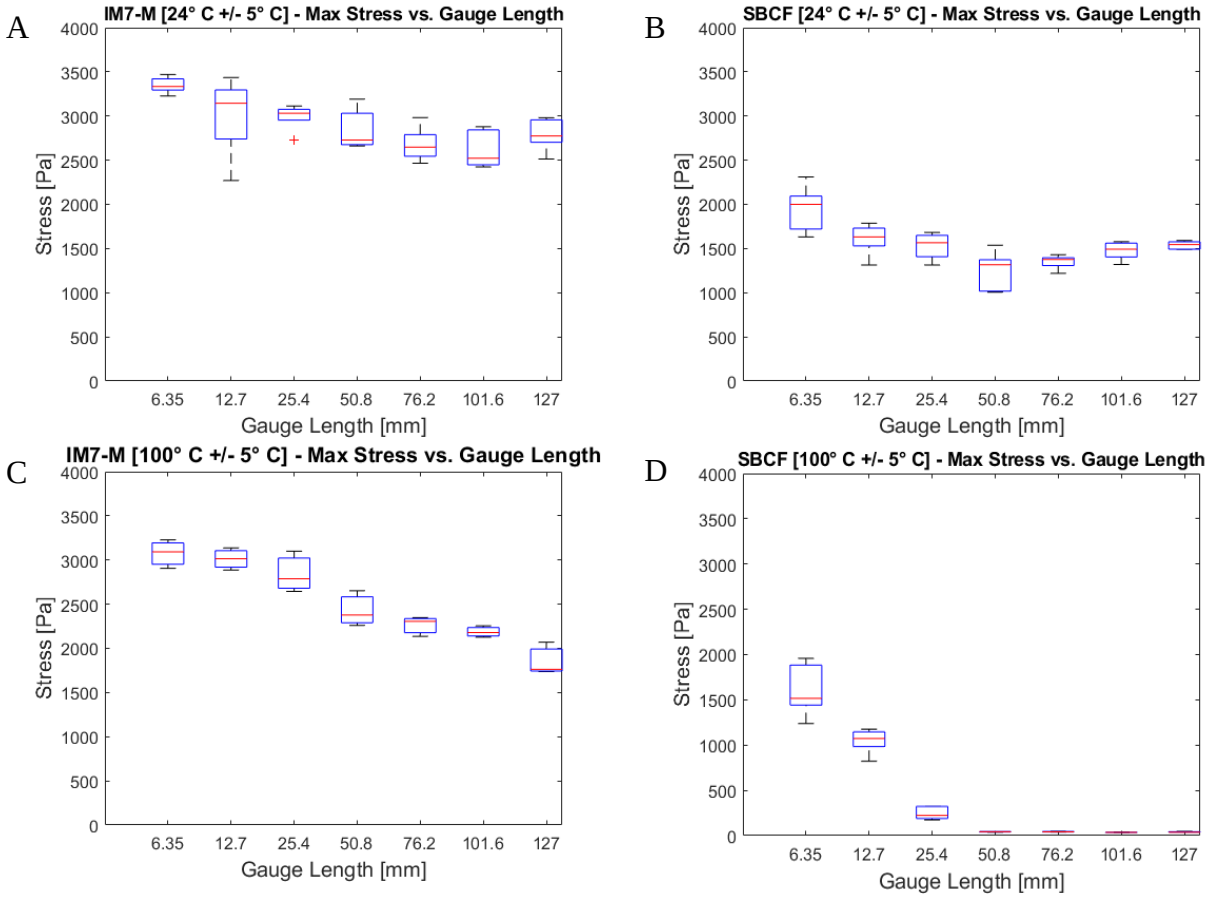

Figure 3.7: (A) Room temperature load vs. stress boxplots of continuous and (B) MSU SBCF (C) Elevated temperature load vs. stress boxplots of continuous and (D) MSU SBCF

Figure 3.8 A displays a curve fit that compares the performance of each type of fiber at room and elevated temperature. It was notable that the disparity in maximum load and associated tensile strength for continuous fiber at room and elevated temperature was almost indistinguishable. However, the tensile load for SBCF at room temperature was consistently much lower than continuous fiber. Upon heating, SBCF exhibited a comparable tensile behavior to both continuous fiber and room temperature SBCF at smaller gauge lengths. However, there was a

severe drop in tensile strength and peak load as the gauge length increased. This change was attributed to the material characteristics of SBCF, where the fiber became discontinuous at 25.4 mm. The leveling out of the maximum load required in tension was evident in Figure 3.8 which serves as an indicator of this transition. Figure 3.8 B is a reference to prior work carried out in this project that involved testing SBCF with a mean fiber length of 50.8 mm and IM7-G continuous fibers supplied by Hexcel Corporation [2]. Two notable differences were observed between Figures 3.8 A and B. Firstly, the IM7-M continuous fibers exhibited notably higher peak forces when compared to IM7-G continuous fibers. This disparity can be attributed to the M sizing, which had a higher weight percentage of 1.86% compared to 0.25% despite both fibers being identical [15, 20]. Secondly, the green curves represent a comparison of mechanical properties between MSU SBCF and Hexcel Legacy SBCF at an elevated temperature of 100 °C. The MSU SBCF, with a mean fiber length of 30 mm, displays a noticeable decline to almost zero at a much smaller gauge length than Hexcel Legacy SBCF with a mean fiber length of 50.8 mm [2,15]. This enhancement is advantageous as it improves formability, that is why a shorter mean fiber length is desirable for SBCF.

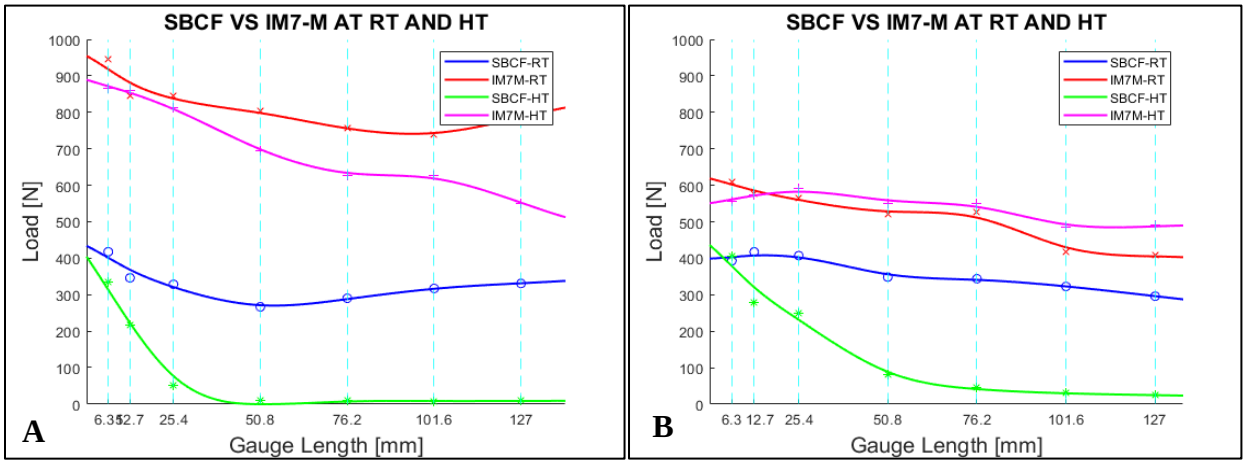

Figure 3.8: Load vs. gauge length plots at room (RT) and elevated (HT) temperatures of (A) MSU SBCF and continuous materials and (B) Hexcel Legacy SBCF and continuous materials[2]

Conclusions

This experiment aimed to compare the tensile properties of SBCF and continuous carbon fiber tows, and to investigate the effect of gauge length and temperature on the tensile strength of these materials. The results showed that the increasing gauge length had a significant impact on the tensile strength of both SBCF and continuous carbon fiber due to the increased number of fiber break points or natural flaws in the fibers. Additionally, the elevated temperature contributed to lower peak forces due to the loss of functionality of the sizing in the SBCF. Comparing the impact of peak load versus displacement, it can be observed that MSU SBCF, with a mean fiber length of 3 cm, had much lower peak forces under smaller gauge lengths as opposed to Hexcel's SBCF with a mean fiber length of 5 cm. Both materials exhibited close to ten times lower peak forces than continuous carbon fiber. Interestingly, as the gauge length exceeded the mean fiber length for the SBCF, stresses plummeted to near zero MPa. These findings indicate a clear path towards reducing vacuum pressure when utilizing SBCF to increase formability.

CHAPTER FOUR

TENSILE PROPERTIES OF STRETCH BROKEN CARBON FIBER PREPREG

Contribution of Authors and Co-Authors

Conference Proceeding in Chapter 4: Tensile properties of stretch broken carbon fiber prepreg

Author: Dalton Nold

Contributions: Methodology, Data curation, Formal analysis.

Co-author: Dilpreet S. Bajwa

Contributions: Conceptualization, Supervision, Visualization.

Co-author: Douglas Cairns

Contributions: Project administration, Conceptualization, Funding acquisition.

Co-author: Roberta Amendola

Contributions: Conceptualization.

Co-author: Cecily Ryan

Contributions: Conceptualization.

Co-author: Christopher Ridgard

Contributions: Methodology, Resources, Validation.

Manuscript Information

Dalton Nold, Dilpreet S. Bajwa, Douglas Cairns, Roberta Amendola, Cecily Ryan, Christopher Ridgard

Conference proceeding in Chapter 4: Tensile Properties of Stretch Broken Carbon Fiber Prepreg

____ Prepared for submission to a peer-reviewed conference proceeding
____Officially submitted to a peer-reviewed conference proceeding
____ Accepted by a peer-reviewed conference proceeding
_X_ Published in a peer-reviewed conference proceeding

Publisher: SAMPE
Published: Jan 2023

Introduction

Composites have become immensely popular in the aerospace industry due to their robustness and lightweight material properties. As an example, the Lockheed Martin F-22 fighter jet consists of 24% composites by weight. This includes 11% in the aft fuselage and 35% in the wings including the skins [27]. This reduction in weight allows the fighter jet to consume less fuel. The utilization of composites incorporating (PAN) derived carbon fibers can enhance the structural integrity of an aircraft while simultaneously reducing its weight. This leads to notable improvements in fuel efficiency, corrosion resistance, and flight maneuverability. Additionally, the mechanical properties of these composites, including strength and stiffness, are on par with those of titanium which is a much denser material. [2,3]. A major issue with implementing carbon fiber composites into an aircraft structure is the loss of versatility in forming a part that has sharp corners and deep drawn geometries. To combat this issue, the carbon fiber prepreg needs to undergo some plastic deformation in the fiber direction to fit the mold under a much lower pressure. This is accomplished by altering the continuous fiber into a discontinuous fiber prepreg where the broken fibers are randomly distributed along the length and width of the material. This allows the fibers to slide against each other in the fiber direction while the matrix is viscous enough to allow the prepreg to form and consolidate. This version of carbon fiber prepreg is known as stretch broken carbon fiber (SBCF) prepreg which when cured, retains up to 95-100% strength and stiffness of continuous carbon fiber [4,5,8-12]. Montana State University has developed a proprietary technology to manufacture SBCF.

This study involved the determination and graphical representation of the true stress-true strain relationship in a tensile test for single-tow prepreg material comprising of SBCF. The experiment was carried out at an optimized temperature that facilitated efficient resin viscosity formation for formability.

Traditionally, stress is computed by dividing an applied force by a specific area, resulting in engineering stress. However, this approach is prone to error due to Poisson's ratio, a common characteristic of most materials. Poisson's ratio describes the tendency of a material to expand or contract perpendicularly to the direction of tension or compression [28]. Refer to Figure 4.1 below for a visual representation of this phenomenon.

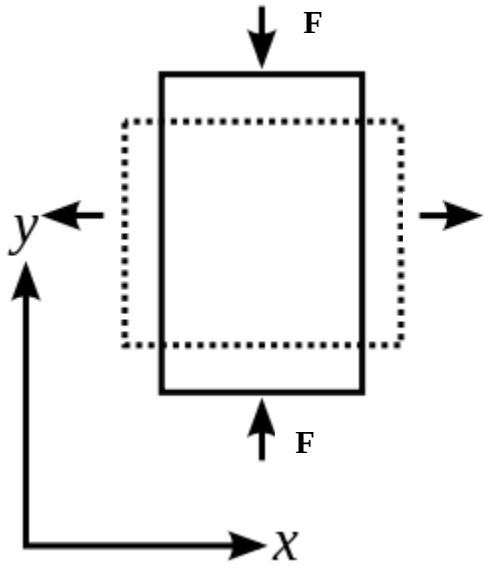

Figure 4.1: Poisson’s ratio

As a material’s cross-sectional area tends to change throughout a tensile test due to the deformation, tracking the materials instantaneous areal change can be complicated. This instantaneous change in force with respect to area is called true stress and depicts a more realistic elastic modulus of the material. The true strain can be incorporated by converting the engineering

strain data on to a log scale [7, 29]. In this chapter, the increasing displacement resulted in a reduction in fiber areal weight that reduced the samples cross-sectional area in real time. It was hypothesized that the discontinuous fibers would not strain harden in response to stretching.

Materials

The fibers used in this test were obtained from Hexcel Corporation and consisted of 12k IM7-G fibers. The fibers from the spools were sent through the stretch breaking machine and immediately had resin film applied to obtain stretch broken prepreg that consisted of ten individual tows to form a ribbon of stock material (DTP). The prepreg made for these tests used Solvay CYCOM® 977-3 (Solvay S.A., Neder-Over-Heembeek, Brussels, Belgium) and Hexcel HexPly® 8552 epoxy resin systems. The prepreg ribbon produced was then consolidated on a machine from Century Design, Inc. (CDI, San Diego, CA, USA) where it was subjected to various rollers and pads that applied heat and pressure displayed in Figure 4.2. The prepreg was then slit back into single tows of equal widths of 6.3 mm for this study. The prepreg material properties are shown in Table 4.1.

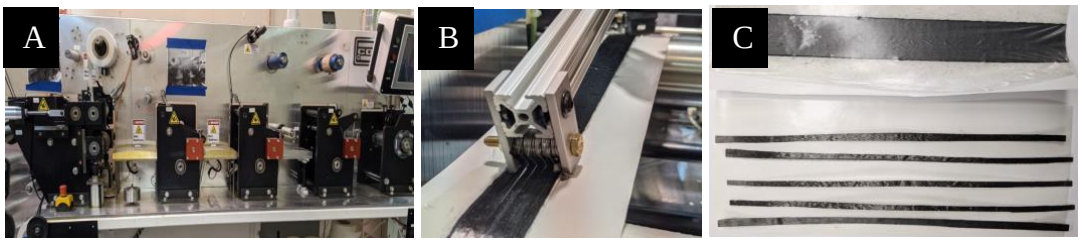

Figure 4.2: (A) Prepreg compaction (B) Slitting process (C) Material before and after going through CDI machine

Table 4.1: Prepreg material properties [2]

SBCF Single Tow Properties		
Resin type	**977-3**	**8552**
Tow weight (gsm)	117.9	111
Estimated fiber count (+/- 300)	9,700	9,700
Filament diameter (mm)	0.0052	0.0052
Resin %	33	38.02

Resin percentages were calculated in a vacuum filtration process where an even mixture of N-methyl pyrrolidone (NMP) solvent and pure acetone washed the resin away. Changes in the weight before and after treatment helped to determine the amount of resin in the material on a volume basis and is portrayed in Figure 4.4.

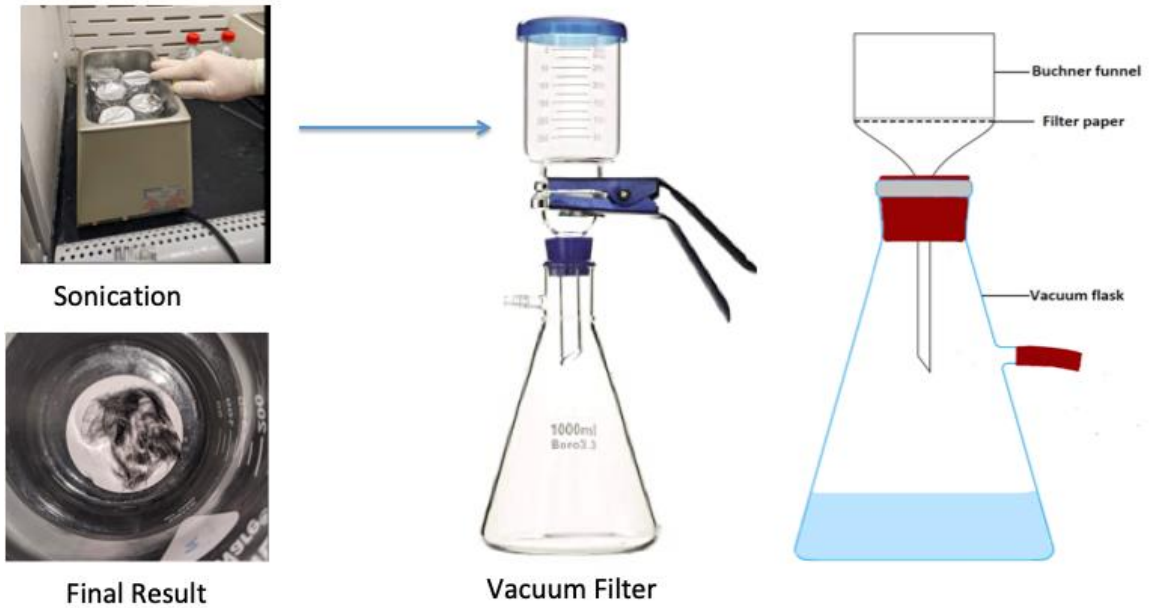

Figure 4.4: Vacuum filtration methodology

Cardboard tabs were applied at the ends of the samples using a fast-setting ethyl cyanoacrylate glue that allowed the teeth of the clamps to prevent slippage as tension was applied. A sample gauge length of 127 mm was exercised between the cardboard tabs. The test sample was loaded into a Mark 10 ESM 303-universal testing machine fitted with a custom heat enclosure to help apply uniform convectional heat to the test sample via analog controlled heat gun.

Test Methodology

Utilizing a load cell with a load capacity of 100 N, the Mark 10 apparatus was retrofitted to facilitate the measurement of both load and deflection parameters. These values were utilized in the computation of accurate stress versus strain relationships, as shown in Figure 4.5.

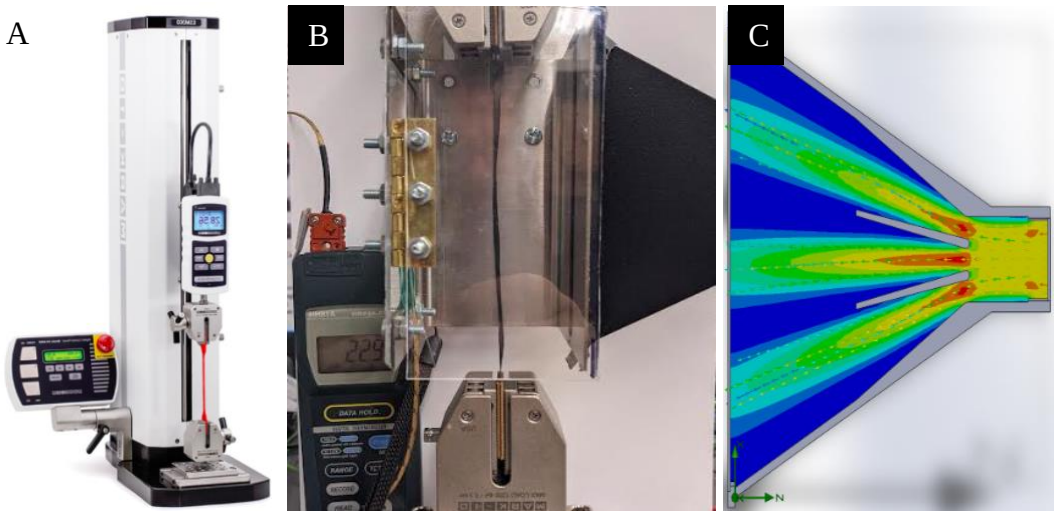

Figure 4.5: (A) Mark-10 ESM 303 (B) Custom heat enclosure (C) Heat duct distribution model

A Fluke Thermal Imager was used to track the exact temperature of the sample and bring the sample temperature to the desired debulking temperature for each resin type. The temperatures were determined by a simulation software known as Raven from Convergent Engineering (Convergent Engineering, Newberry, FL, USA) which would determine an appropriate viscosity

that would increase ease of formability at atmospheric pressure. The 977-3 prepreg samples were tested at 135℃ and the 8552 prepreg samples were tested at 121℃. The two resin systems are both used in similar military and other applications but have different rheological and mechanical performance characteristics which are used by end users to determine the optimum material for a given application. 977-3 has a lower viscosity than 8552 and is less reactive, which is why different temperature and time profiles are appropriate for the processing of each in the work presented herein. A basic criterion used to determine the forming temperatures was to estimate the highest temperatures at which a low resin viscosity could be maintained for sufficient time for forming to occur without advancing the material and increasing the viscosity before forming is able to take place. This is called the debulking temperature and Figure 4.6 illustrates this for both resin systems.

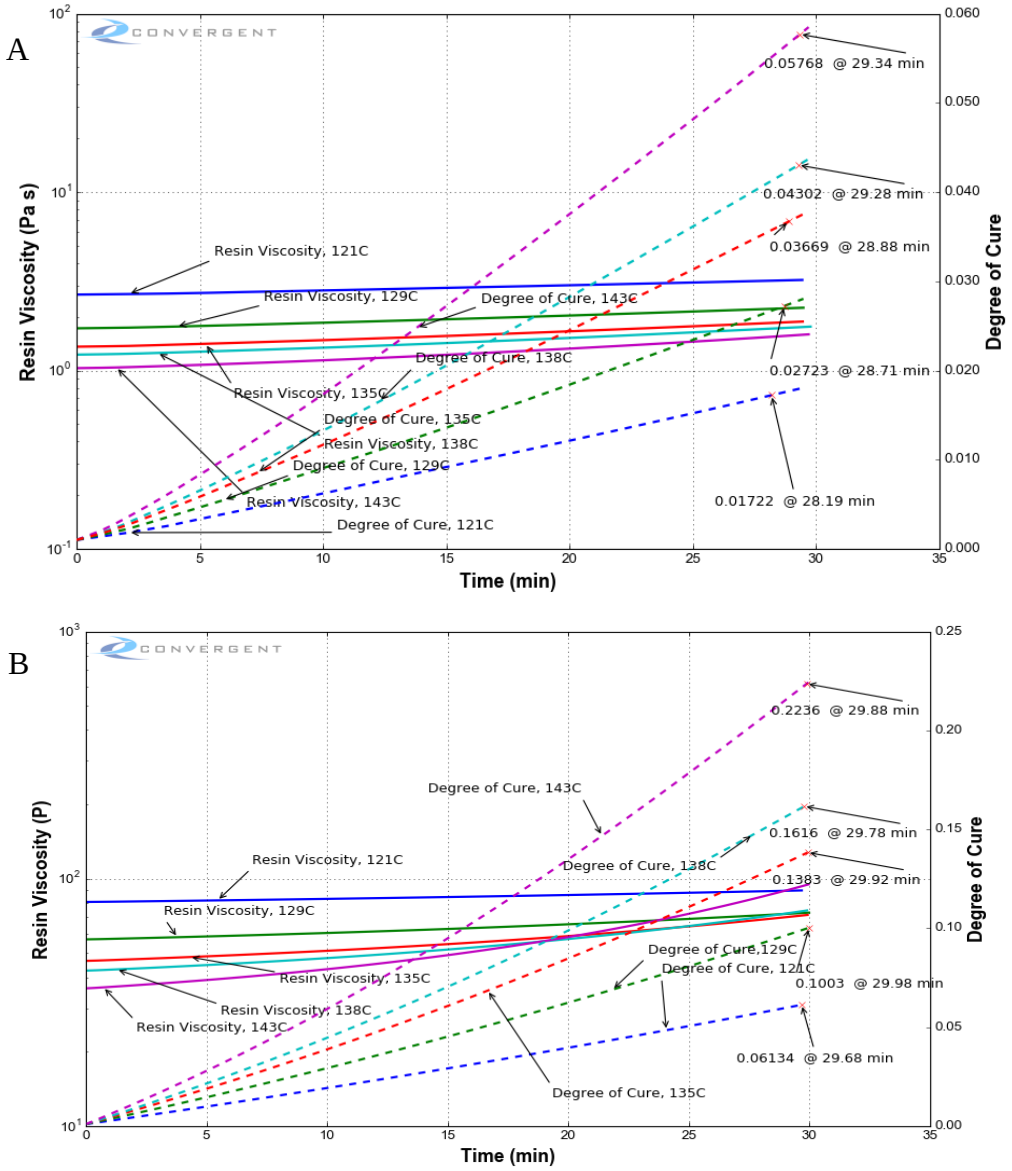

Figure 4.6: (A) Debulking simulation for 977-3 resin; temperature chosen from red curves (B) Debulking simulation for 8552 resin; temperature chosen from blue curves

Figure 4.7 is a screenshot of the thermal image reading which guided the user when to start the test once the sample reached its desired temperature. It is worth noting that the experimental configuration employed herein bears a resemblance to the test apparatus utilized in Chapter Three.

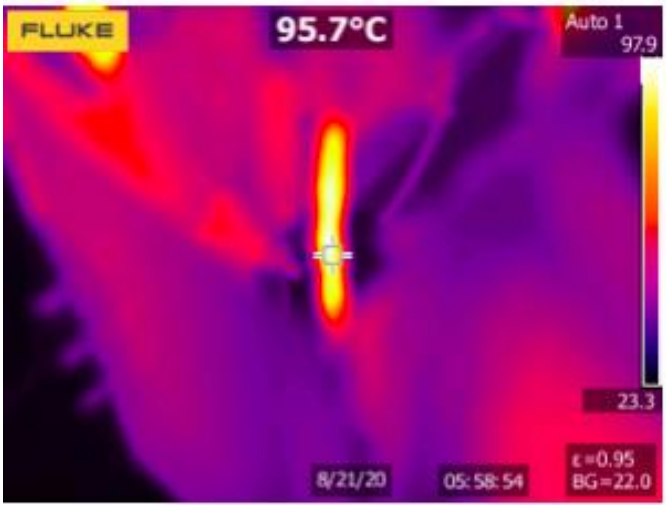

Figure 4.7: Real time thermal image reading of test specimen

To calculate true stress, the force must be divided by the cross-sectional area. The instantaneous areal cross-section was measured where the sample experienced the most displacement. To measure the thickness, a high resolution Mitutoyo digital micrometer was utilized. For measuring width, a Canon Rebel t4i camera was used to take a picture of the tested sample next to a Mitutoyo scale ruler. This setup is shown in Figure 4.8. Following this procedure, a picture of the sample was taken with the known scale in the frame and converted to the pixel distance in millimeters shown in Figure 4.9.

Figure 4.8: Picture of a sample taken using a Canon Rebel t4i camera

Several pictures were taken after the test and then analyzed using the ImageJ software (National Institutes of Health, Bethesda, MD, USA) to collect data on the new width of the tested sample.

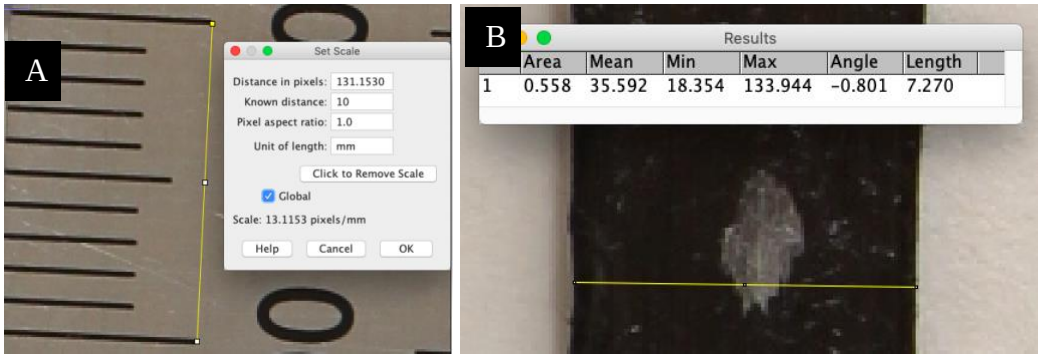

Figure 4.9: (A) ImageJ software for converting pixels into metric length (B) Applies metric distance to known pixel length to measure the sample's width

Several pictures were taken after the test and then analyzed using the ImageJ software (National Institutes of Health, Bethesda, MD, USA) to collect data on the new width of the tested sample.

To determine true stress, 35 samples were divided into groups of five samples. Each individual sample set of five was stretched to the same length where the true stress was calculated and then averaged into a single data point. These individual sample sets were increased in increments of 1 mm (i.e. ΔL=1, 2, 3, 4, 5, and 6 mm) using a crosshead speed of 6.30 mm/min.

The testing showed that the maximum peak force occurred at less than 1 mm of stretching. With this, true stress vs. strain data was collected at these points as well to provide a more accurate peak stress value. Table 4.2 tabulates how the samples were divided into seven different data points.

Table 4.2: Sample testing approach

Samples	ΔL
1-5	ΔL at Peak force
6-10	1 mm
11-15	2 mm
16-20	3 mm
21-25	4 mm
25-30	5 mm
31-35	6 mm

Once the peak forces were acquired, averages of the true stress were taken and used as a single data point on the true stress/strain curves shown later in Figures 4.12-4.14. Table 4.3 illustrates how to convert the local engineering strain to logarithmic or "true" strain [7]. The logarithmic strain estimated the correct measure of the final strain during deformation in a localized series of increments, which also considered the influence of the strain paths.

Table 4.3: Equations for true stress and strain [7]

P = load	P = load
A_o = initial cross-sectional area	A_i = instantaneous cross-sectional area
Engineering Stress = $s = P/A_o$	**True Stress = $\sigma = P/A_i$**
l_o = initial length of gauge section	l_i = instantaneous gauge length
l = length of deformed gauge section	l_o = initial length of gauge section
$\Delta l = l - l_o$ = change of length of gauge section	
Engineering Strain = $e = (l-l_o)/l_o = Dl/l_o$	**True Strain = $\varepsilon = \ln (A_o/A_i) = \ln (l_i/l_o)$**
Converting Engineering Stress to True Stress:	**$\sigma = s(1+e)$**
Converting Engineering Strain to True Strain:	**$\varepsilon = \ln(1+e)$**

Since the SBCF prepreg would have different strain regions along the length of the tow, the distortion on the markings on the tow determined where the highest strain occurred. This was the targeted region where the area was measured for true stress and true strain and is shown below in Figure 4.10.

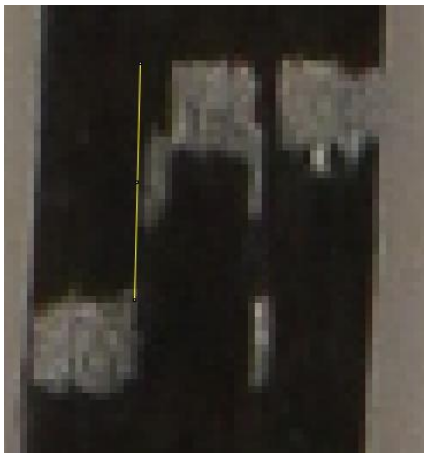

Figure 4.10: Localized strain measurement using ImageJ software

Results and Discussion

In a forming environment, pressures are induced perpendicular to the fiber direction to help the material form in the mold. However, testing this material in a one-dimensional tensile loading depicted a more accurate representation of the mechanisms of how the material behaved under said loading. Fundamental understanding of the material in prepreg form can further help to improve the quality of cured carbon fiber composites. In this experiment, it was discovered that when a tensile reading from the load cell hits a global maximum, it was not the individual fibers that were moving against each other. This is illustrated in Figure 4.11, where the fiber movement is non-homogeneous, and the fibers tend to cluster and slide along one or more shear planes at a time.

Figure 4.11: Fiber movement of samples after stretching

Figures 3.12 and 3.13 display similar strain softening behavior, which was an outcome of the material's heterogeneity. The presence of the shear planes validated why the true stress and strain show a strain softening behavior for both resins. At high temperatures the resin acted as a lubricant due to its low viscosity. Figure 3.14 illustrates the similarity of the two curves side-by-side at their different logarithmic strains.

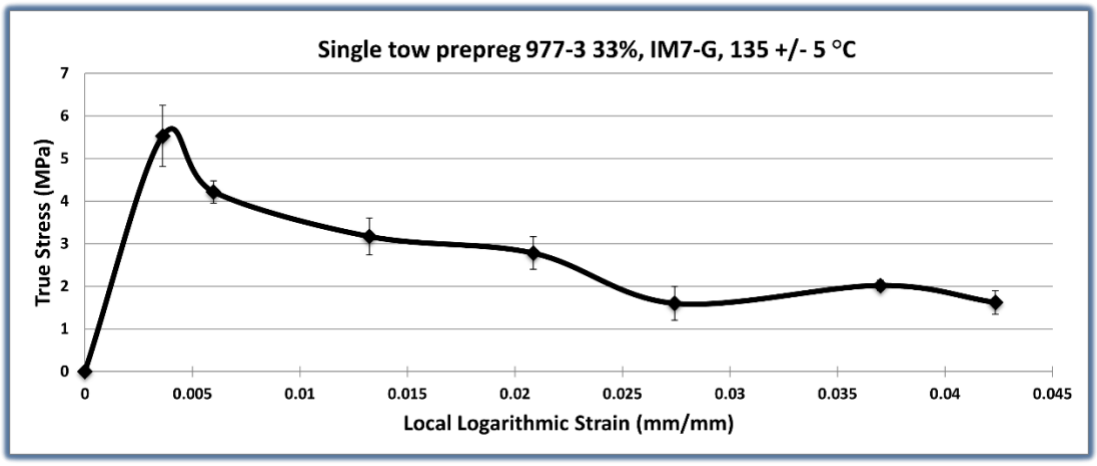

Figure 4.12: True stress vs. logarithmic strain of IM7-G 977-3 MSU SBCF prepreg

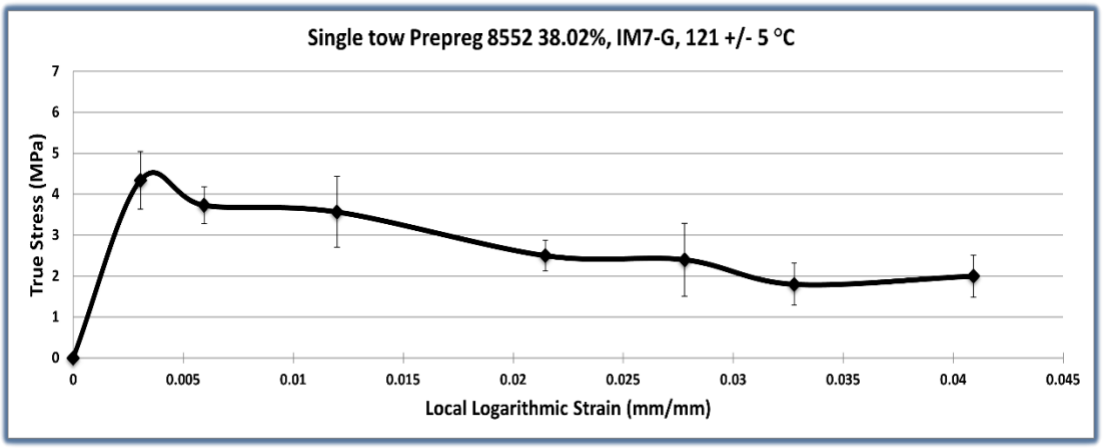

Figure 4.13: True stress vs. logarithmic strain of IM7-G 8552 MSU SBCF prepreg

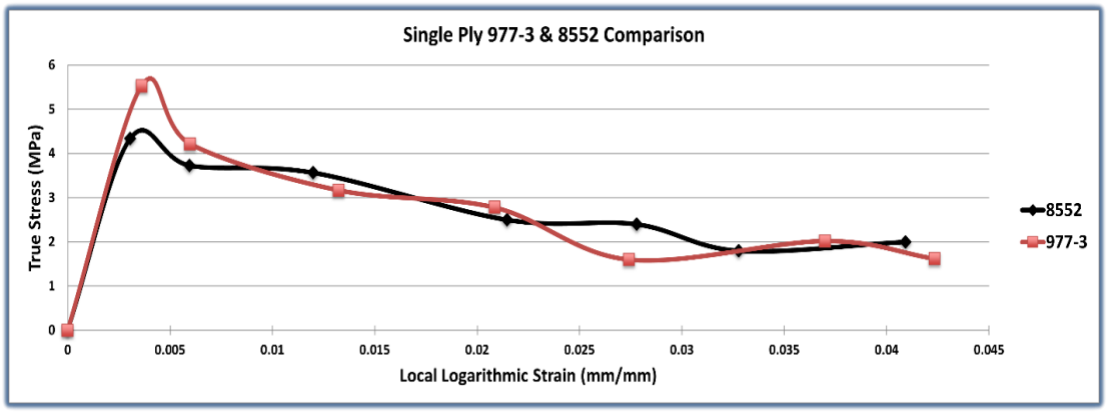

Figure 4.14: Side by side comparison with 977-3 and 8552 resin systems

From the data provided, the material became weaker in the plastic region before the load was transferred to another shear plane, which allowed the stress in the material to plateau. As more strain was applied, this process repeated as stress deteriorated. Formability in the fiber direction is extremely effective due to the small peak stresses of 4-6 MPa for both resin types in the 33% - 39% range by volume. With the help of transverse loading using vacuum pressure in the curing cycle, it was expected that these values may even be reduced further. If strain hardening was present, forming stresses would increase as the area of the SBCF tow decreased due to better alignment of the fibers, thus making the material more difficult to form. Although resin percent by

volume does affect these forming limits, it had been determined that these percentages were optimal for a final cured material [4].

Further research was conducted of a quasi-isotropic layup of $[0/+45/-45/90]_S$ to investigate if the strain softening behavior would be obstructed by the shear forces of multiple plies oriented away from the applied loading.

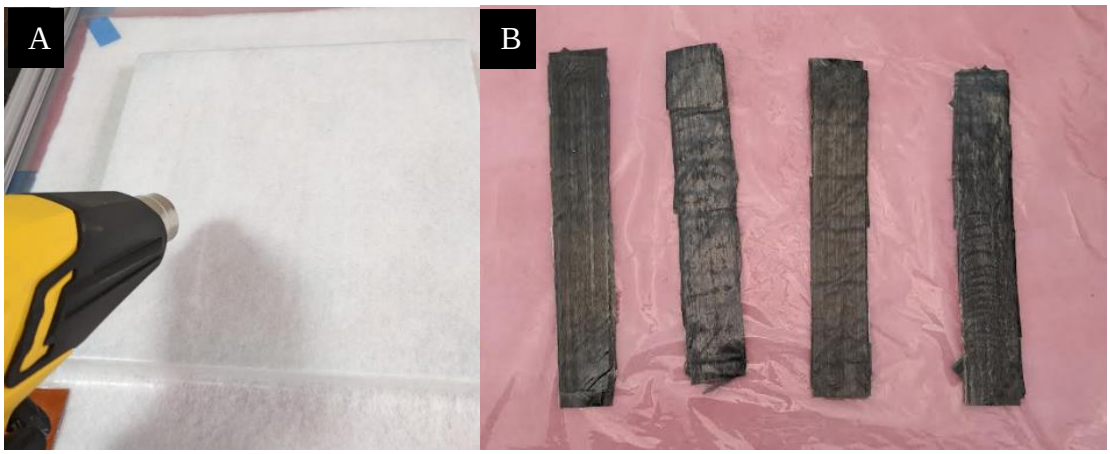

Figure 4.15: (A) Heat gun/vacuum consolidation (B) Prepreg layup $[0/+45/-45/90]_S$

Figure 4.15 A and B depict the layups of specimens and their consolidation by applying heat and pressure. Afterward, the specimens were trimmed to a width of 12.7 mm and equipped with cardboard tabs. Subsequently, the same design of experiment utilized for the single tow material was employed for these samples. The same 977-3 prepreg was utilized, and each data point was averaged across only two samples.

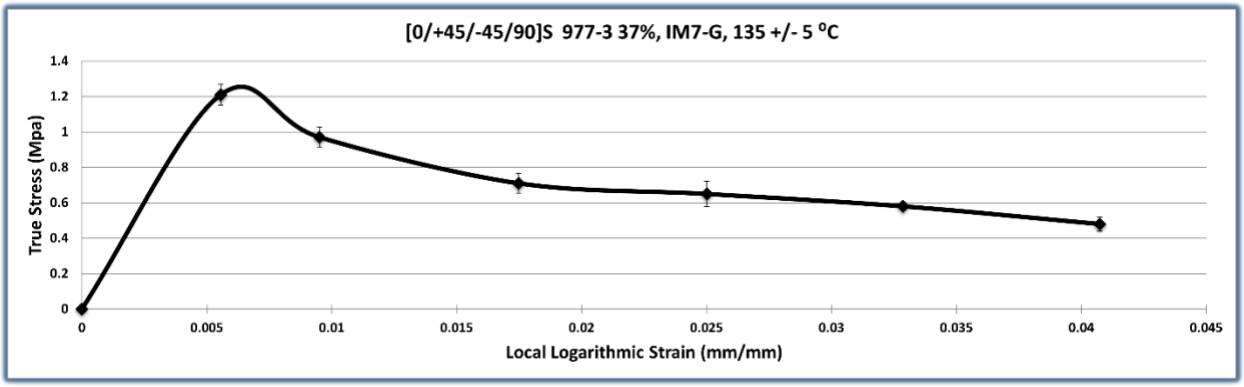

Figure 4.16: True stress vs. true strain of $[0/+45/-45/90]_S$ 977-3 prepreg layup

This preliminary data shown in figure 4.16 ascertains that the shear forces between the plies do not affect the strain softening behavior and was indeed still present.

Conclusion

This experimental investigation involved the characterization of true stress and true strain of single tow MSU SBCF prepreg at elevated temperatures of 121 +/-5 ºC for 8552 resin and 135 +/-5 ºC for 977-3 resins. The test was conducted using a one-dimensional tensile test at a constant displacement rate of 6.3 mm/min. The results indicated that the SBCF prepreg experienced strain softening behavior when using 8552 and 977-3 epoxy resin systems. This observation was confirmed by the presence of shear planes in the tensile test samples after testing had occurred. Notably, the addition of more plies to the test sample at different fiber orientations did not affect the strain softening behaviors observed under uniaxial loading conditions.

CHAPTER FIVE

DETERMINING FORMING PROPERTIES OF STRETCH BROKEN CARBON FIBER PREPREG USING A NOVEL FORMING FIXTURE

Introduction

One of the key drivers of SBCF's high value proposition in the composites manufacturing industry lies in its unique capability to fabricate complete laminates through the utilization of vacuum pressure as the sole method of compaction [16]. This technology offers momentous advantages in terms of manufacturing time savings and productivity optimization, applicable not only to the production of aircraft structures, but across a wide spectrum of industries engaged in fiber composite manufacturing. One of the major hurdles encountered in the SBCF manufacturing process pertains to comprehending the tool geometry's impact on the peak forces essential for surpassing the static friction between the fibers and the matrix. To surmount this challenge, an innovative forming fixture was devised and constructed, which facilitated a systematic and iterative testing approach for the rapidly evolving SBCF production being researched. This highly adaptable forming fixture affords precise control over temperature and tool geometries [14, 21]. Figure 5.1 depicts a schematic representation of the underlying principles and operational functionality of the forming fixture.

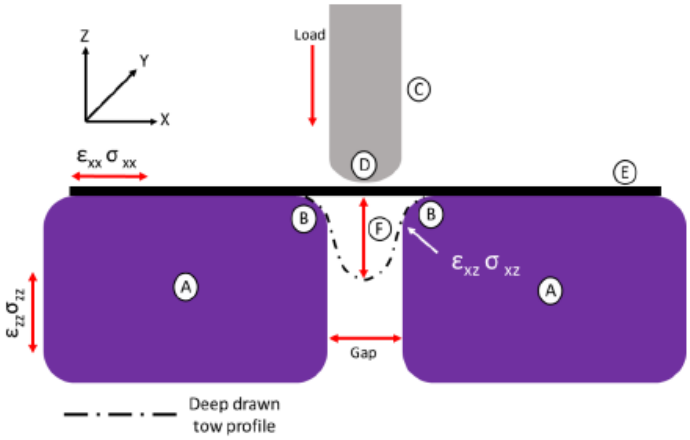

Figure 5.1: Forming fixture test design concept (A) forming blocks, (B) forming blocks radius of curvature, (C) forming tool (“plunger”), (D) forming tool radius of curvature, (E) sample and (F) deep drawing depth [14, 21]

In the continuum model put forth above, the test specimen (E) is subject to the influence of the forming tool (C), which imparts a deep drawn profile between two temperature-controlled blocks (A) known as the "gap" in this study. By analyzing load-displacement data, it became possible to gain insights into the peak forming forces and their interplay with distinct forming tool ("plunger") diameters (D) and varying gap widths.

The initial phase of this study employed a forming fixture to compare the mechanical behavior of single tow prepreg versus the tensile properties of discontinuous carbon fibers provided by Hexcel. The resulting data provided evidence of the concept viability and demonstrated significant disparities between the peak forces of continuous and discontinuous fibers. In this chapter, a design of experiment was executed that employed a larger quantity of MSU SBCF to compensate for the data noise that arise from load cell measurements due to the low peak forces generated by a limited number of discontinuous fibers (at elevated temperatures). The hypotheses tested in this chapter proposed that increasing the gap between the heated blocks would result in lower peak forming loads due to the greater number of fiber break points along the

gauge length. Additionally, it was postulated that enlarging the plunger diameter would raise the peak forming loads by enhancing the contact area between the tool and the ply, leading to more friction.

Materials

The fibers used in this test were 12k IM7-G fibers sourced from Hexcel Corporation. As discussed in Chapter Two, the carbon fibers from the spools were sent through the stretch breaking machine and immediately had resin film applied to obtain stretch broken prepreg that consisted of ten individual tows that formed a ribbon of stock material (DTP). The prepreg manufactured for these tests used Solvay CYCOM® 977-3 (Solvay S.A., Neder-Over-Heembeek, Brussels, Belgium) and Hexcel HexPly® 8552 epoxy resin systems. The prepreg ribbon produced was then consolidated on an Elite M90/100 Fusing machine from Reliant Machinery Ltd (Luton, Bedfordshire, UK) as shown in Figure 5.2 A, where it was subjected to various rollers and pads to apply heat and pressure. A summary of the pertinent prepreg material properties is presented in Table 5.1.

Figure 5.2: (A) Prepreg fusing compaction machine (B) Prepreg cut into sample length (C) Prepreg tabbed and ready for testing

Table 5.1: Prepreg material properties [2]

SBCF Tow Properties		
Resin type	**977-3**	**8552**
Tow weight (gsm)	110	110
Estimated fiber count (+/- 300) *	9,700	9,700
Filament diameter (mm)	0.0052	0.0052
Resin %	36	37
Debulking / testing temperature (+/-5 ºC)	135	121

*Fiber count for individual tow, test samples included 10 tows

Test Methodology

Once necessary quality control parameters were tabulated, the material was ready to be prepared into test samples. Cardboard tabs were applied at the ends of the samples using a fast-setting ethyl cyanoacrylate glue, which allowed the teeth of the clamps to prevent slippage as load was applied. A sample areal gauge length of 203.2 mm x 31.75 mm was used between the cardboard tabs. The test sample was loaded into a Mark-10 ESM universal testing machine (Mark-10, Copiague, NY, USA) with the forming fixture installed. Further details of the forming fixture can be found in previously published papers [8,14]. The temperature within the blocks and plunger were carefully regulated using heater elements to replicate the tool temperature encountered in a debulking process. The plunger was set to operate at a constant displacement rate of 6.3 mm/min, and load-displacement data was captured using the MESUR® software provided by Mark-10. Despite not being depicted in Figure 5.3 B, a 25.4 mm diameter rod with an extrusion of 51 mm

was securely fastened between the force gauge and the plunger to prevent the dissipation of heat into the force gauge. The rod was developed using peek polymer, which conducts heat poorly.

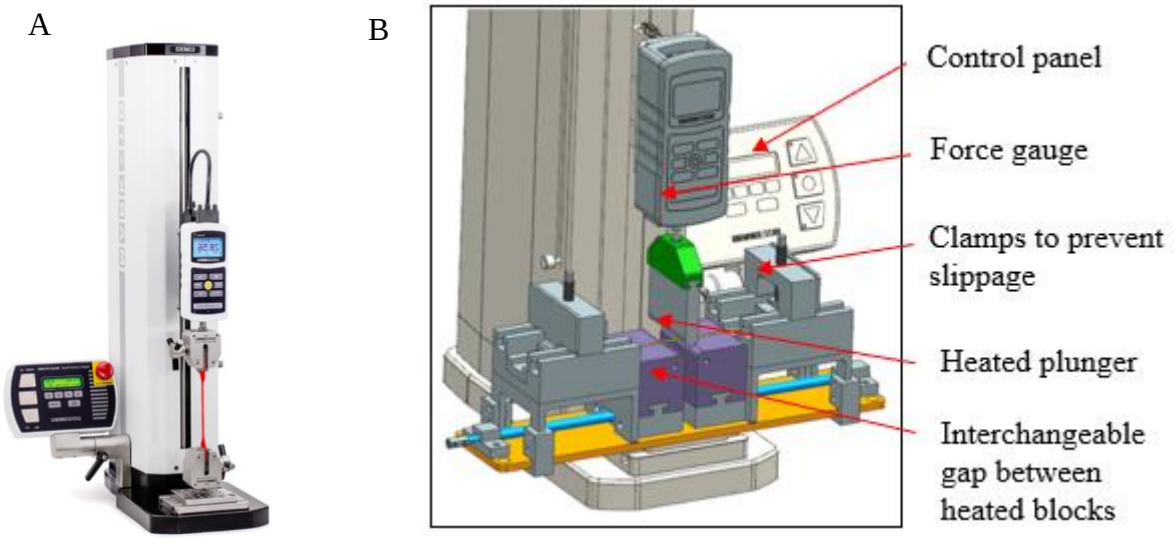

Figure 5.3: (A) Mark-10 ESM 303 (B) Novel forming fixture design model

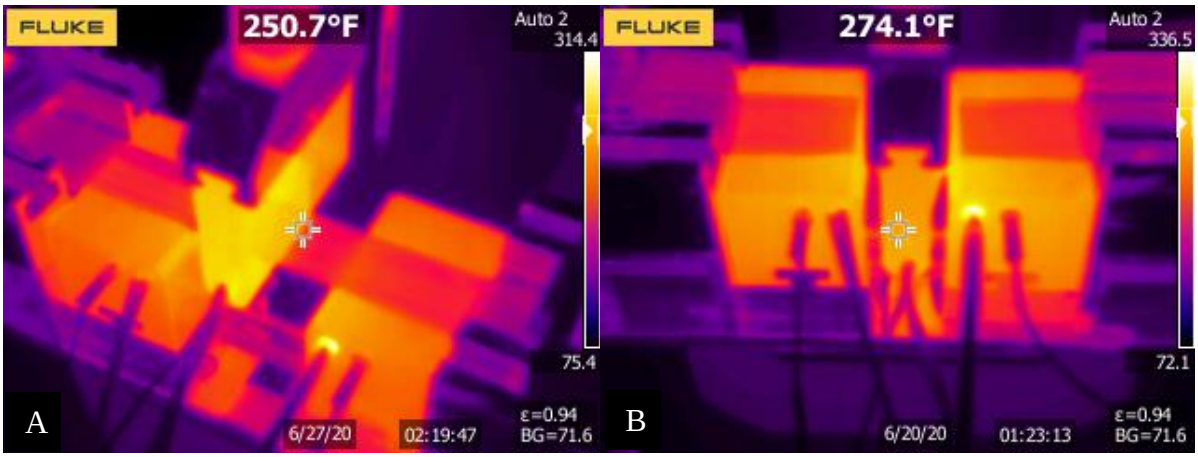

Figure 5.4: (A) Desired temperature for 8552 debulk (B) Desired temperature for 977-3 debulk

A Fluke Thermal Imager was used to determine the exact temperature of the sample and to adjust the sample temperature to the desired debulking temperature for each resin type and verified the J-type thermocouple reading from the heater box. Both the heated blocks and plunger had an emissivity coating for accurate temperature measurements. The temperatures were determined by

a simulation software known as Raven from Convergent Engineering (Convergent Engineering, Newberry, FL, USA) which determined an appropriate viscosity that would increase the ease of formability. The 977-3 prepreg samples were tested at 135℃ (275℉) and the 8552 prepreg samples were tested at 121 ℃ (250 ℉). These temperatures are the dwell temperatures that were selected according to the available viscosity and reactivity data for the respective resin systems. Both resin types were also tested at room temperature to provide clear understanding that peak forces drastically decreased as the resin viscosity decreased. The two resin systems are both used in similar military and other applications but have different rheological and mechanical performance characteristics which are used by end users to determine the optimum material for a given application. 977-3 resin has a lower viscosity than 8552 resin and is less reactive, which is why different temperature/time profiles were appropriate for the processing of each in the work presented herein. A basic criterion used to determine the forming temperatures was to estimate the highest temperatures at which a low resin viscosity could be maintained for sufficient time for forming to occur without advancing the material and increasing the viscosity before forming was able to take place. Figure 5.5 simulates this for both resin systems.

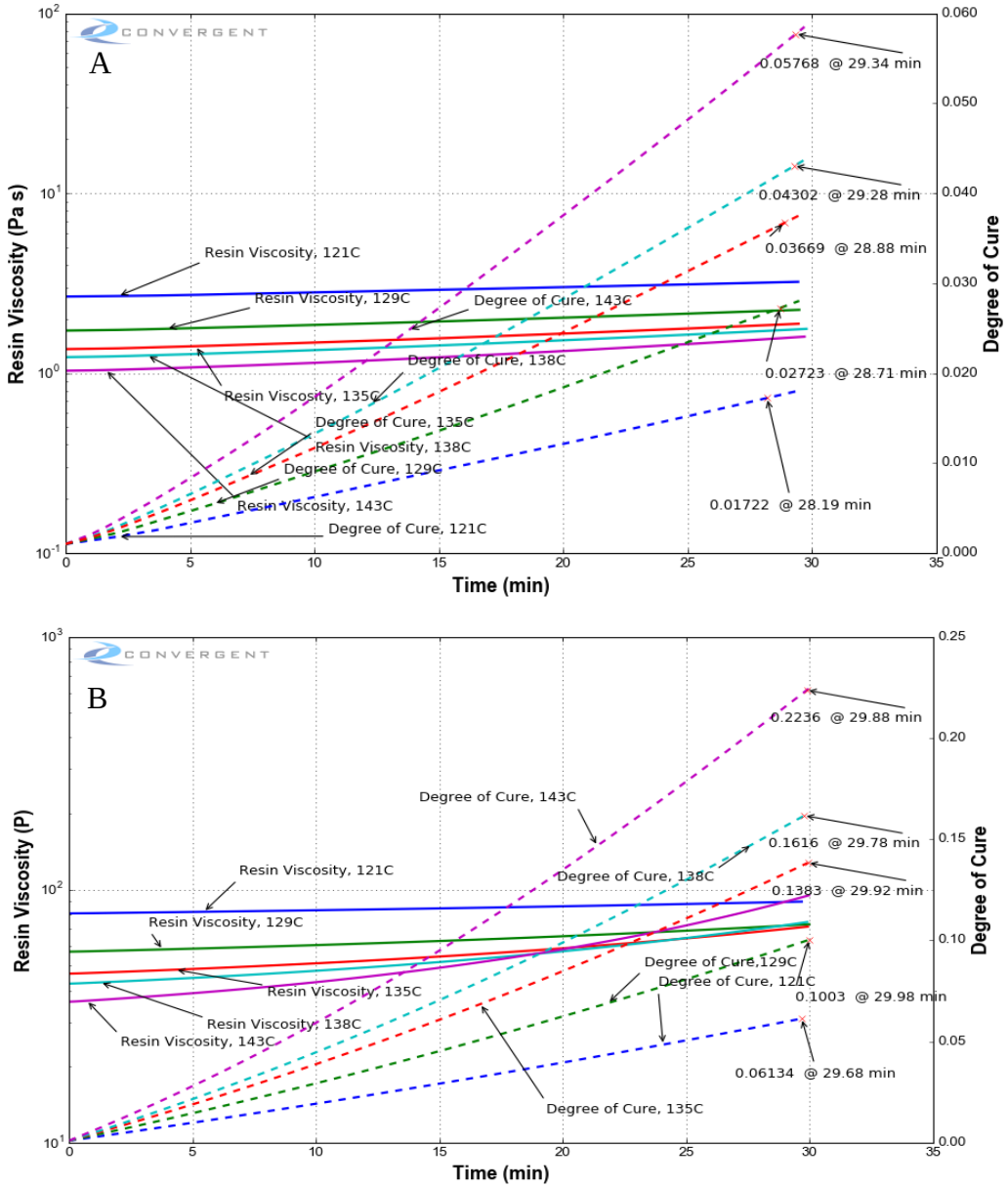

Figure 5.5: (A) Debulking simulation for 977-3 resin; temperature chosen from red curves (B) Debulking simulation for 8552 resin; temperature chosen from blue curves

A meticulously designed test matrix was implemented to examine the impact of diverse gap lengths, ranging from 15.88 mm to 53.98 mm, and distinct plunger diameters, encompassing 12.7 mm, 19.05 mm, and 25.4 mm [14].

Results and Discussion

The importance of this experiment was to understand how the SBCF forms in the forming cycle by undergoing tests with changing parameters and quantifying them by collecting the load versus displacement data. A well-planned design of experiment was formulated to analyze the impact of plunger size and gap width. Upon reaching the peak forming force, the SBCF material experienced strain softening and a modest degree of pseudo plastic deformation due to the displacement of the short-aligned fibers in the fiber direction [13]. Outliers were prudently removed from the data points to eliminate the effect of resin irregularities and unexpected material defects discovered during the data analysis process. These defects encompassed regions characterized by the absence of resin within localized pockets of the material due to the manufacturing process. To minimize the coefficient of variation, these samples were retested in hopes that these defects were not present. Each data point consisted of an average of five samples per data point. In the case of the smallest gap, only one averaged data point could be acquired since the plunger size continued to increase until it exceeded the gap width.

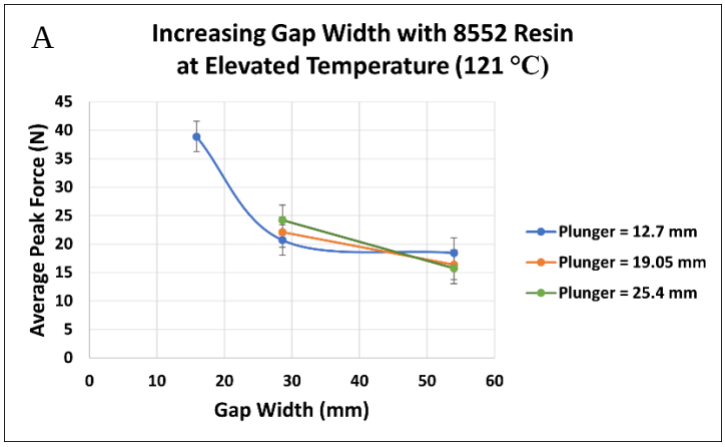

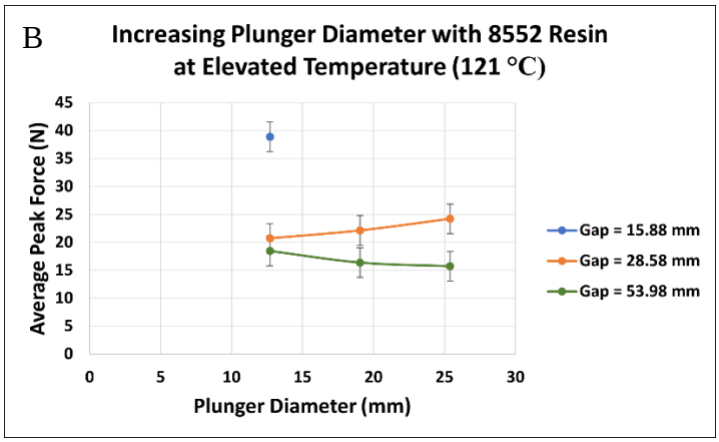

Figure 5.6: (A) Peak force vs. increasing gap width for 8552 elevated temperature (B) Peak force vs. increasing plunger size width for 8552 elevated temperature

In Figure 5.6 A and B, the smallest gap and plunger size produced the largest peak force with 8552 resin of 39 N when undergoing elevated temperature. As expected, the peak force dropped substantially by almost half as the gap width increased. This was predicted due to the increased number of break points of the fiber per unit length of the sample. As it increased, the required amount of force to induce stretch drawing decreased. Regarding the effect of the increasing diameter of the plunger, peak force showed subtle change between the medium and larger gaps. Analysis of variation on this data can be referenced in the Appendices to validate this claim.

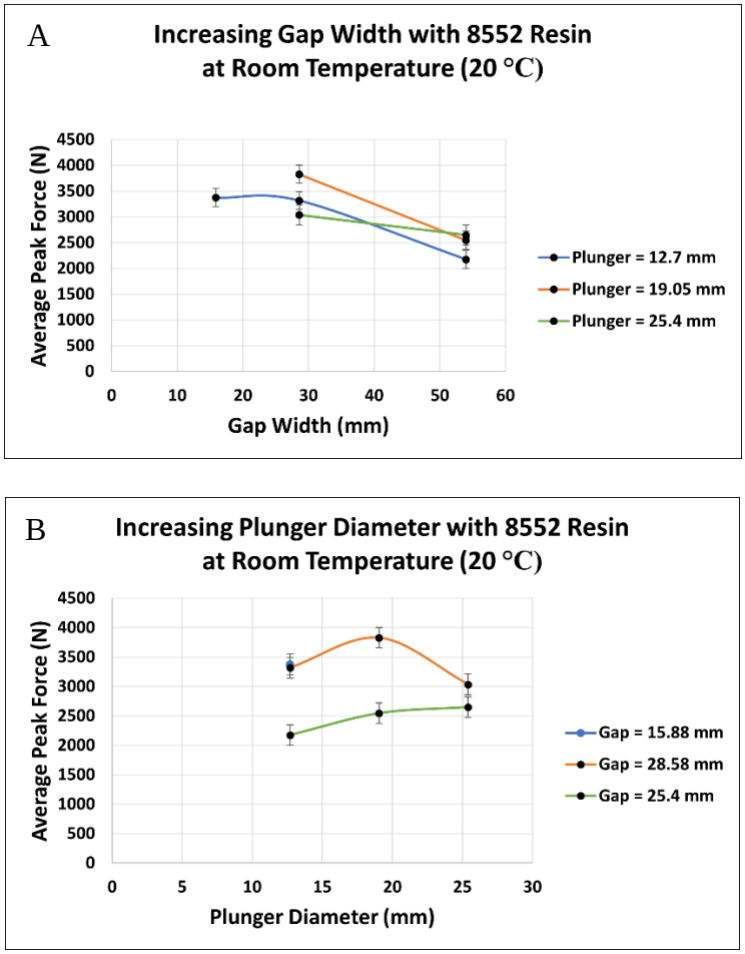

Figure 5.7: (A) Peak force vs. increasing gap width for 8552 room temperature (B) Peak force vs. increasing plunger size width for 8552 room temperature

At room temperature, peak force is 100 times greater than the samples tested at the elevated debulking temperature. As expected, the increasing gap length resulted in a decreasing peak force.

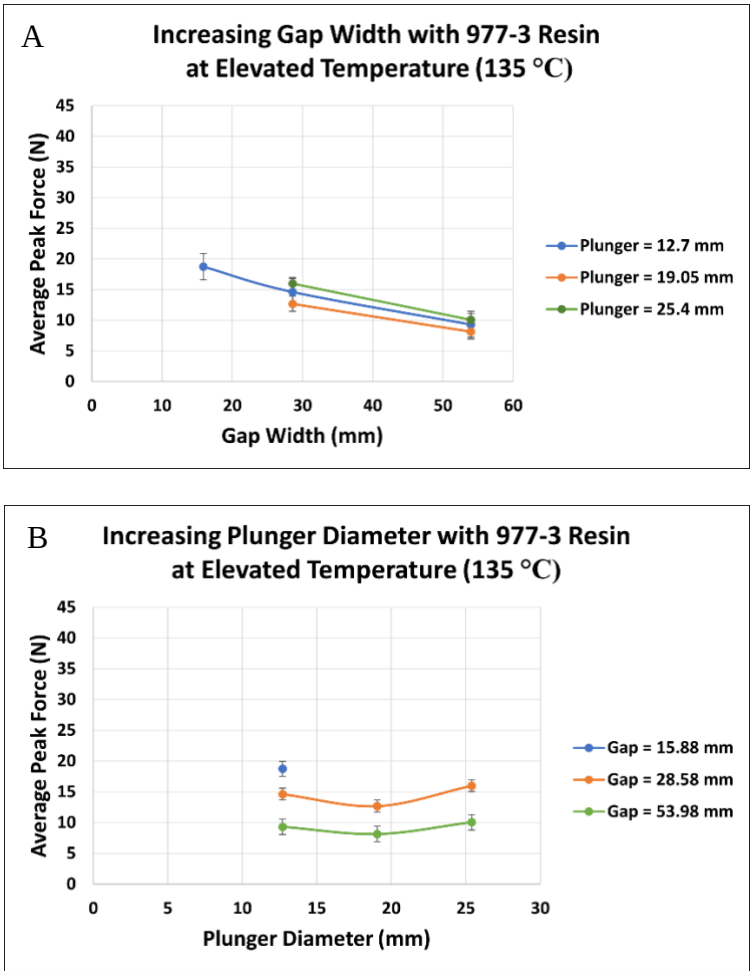

Figure 5.8: (A) Peak force vs. increasing gap width for 977-3 elevated temperature (B) Peak force vs. plunger size for 977-3 elevated temperature

At elevated temperature with 977-3 resin (Fig. 5.8 A and B), the prepreg's response to loading was close to half of the peak force of 8552. The difference in peak force between the smallest plunger size and gap width did not differ much from the medium and large plunger sizes as the gap became larger. Still, when investigating the differential plunger sizes, no important change was observed. Peak forces remained in between 8 to 18.5 N for all plunger and gap sizes. It should be noted that work has been ongoing to improve prepreg quality, which will be the subject of a future journal manuscript. Variations in prepreg quality could have a large effect on

performance in the plunger test and caution needs to be exercised in interpreting results pending the planned addition of further data.

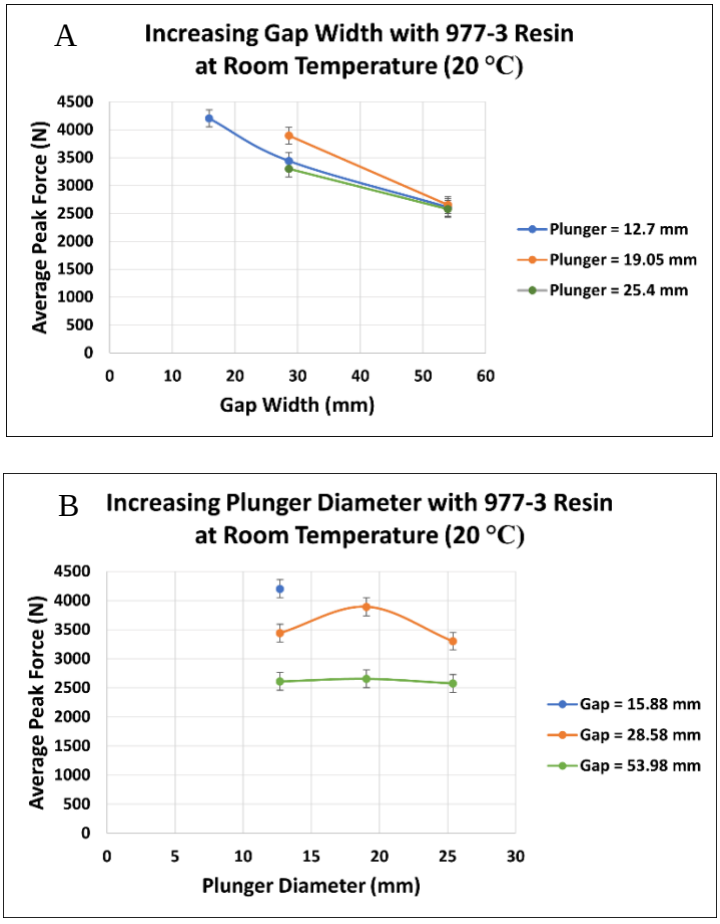

Figure 5.9: (A) Peak force vs. increasing gap width for 977-3 room temperature (B) Peak force vs. increasing plunger size width for 977-3 room temperature

As the samples were observed at room temperature for 977-3 resin, peak forces were again 100 times greater than what was tested at the resin's debulking temperature. Peak force continued to decrease as the gap size increased.

With elevated temperatures and more convoluted tool geometries, 8552 resin required twice the peak force of 977-3 resin to start stretching (Fig. 5.6 and 5.8). However, as noted above, work has been ongoing on optimizing the prepreg manufacturing processes to improve quality and

address problems such as resin advancement which could affect formability. The results reported herein may reflect variations in the prepreg itself rather than indicating that one resin is necessarily 'better' than the other one. At room temperature, the peak force was 100 times greater than what was tested at elevated temperature and underwent brittle failure. This exhibited the importance of debulking the resin to form before properly crosslinking the polymer chains in the resin. It was determined that at elevated and room temperatures, peak forming loads decreased as tool gap increased for both resin types. As discussed earlier, this was because of the increasing number of break points of the fiber per unit length of the sample. As it increased, the required amount of force to induce stretching decreased. For charts with increasing plunger size and elevated temperature, there was not a large difference in peak force, as it was relying more on tool-ply friction which was not changing substantially. At room temperature however, there was a noticeable increase in peak forces at the 28.58 mm size gap and 19.05 mm plunger for both resin types as they then decreased when the 25.4 mm diameter plunger was used. This behavior could be attributed to the unknown mechanical and rheological properties of the proprietary resins. The kinematics of the moving plunger can also influence the peak force of the tows.

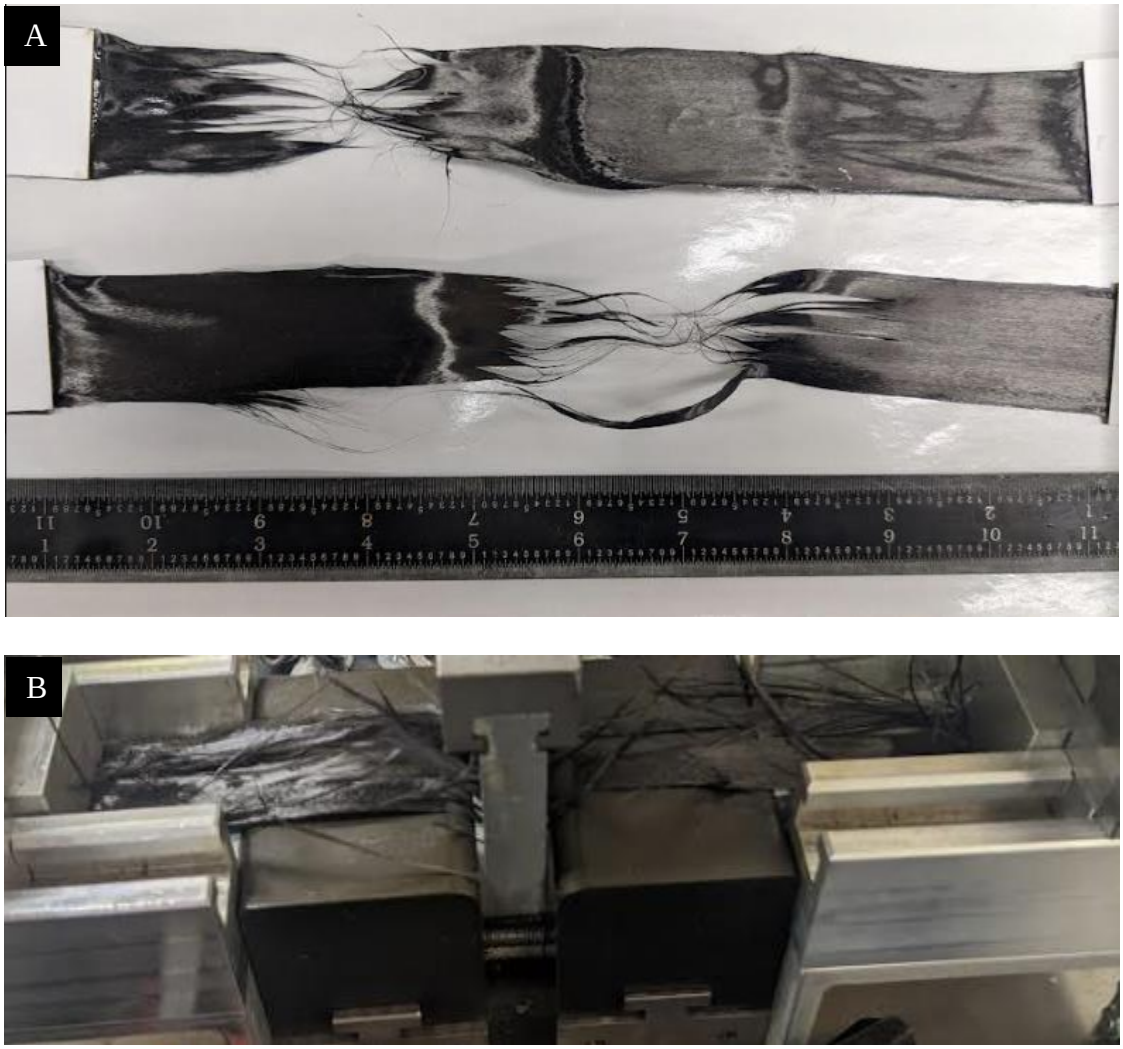

Figure 5.10: (A) Peak force vs. increasing gap width for 977-3 room temperature (B) Peak force vs. increasing plunger size width for 977-3 room temperature

Figure 5.10 depicts radically different failure modes between elevated and room temperatures. Figure 5.10 A shows stretching/failure at high stress points along the gauge length of the tested sample due to drawing. Fig. 5.10 B illustrates brittle failure at all locations of the sample. Both images (Fig. 5.10 A and B) demonstrate matrix dominated failure, which is attributed to differences in the viscosities of the two resins at room and elevated temperatures [8-13].

Further research led to the discovery between whether the forming load was dependent upon the friction between the tool and the ply or if it was between the fibers and the resin that when heated, it acted as a "lubricant' to the fibers as they slid amongst one another. One way this was achieved was to compare the forming results of the SCBF with and without resin. Material with 8552 resin was separated back into ten individual tows and compared to material that was stretch broken from the Bobcat Machine with a 1.86 wt.% of Michelman sizing. The results are tabulated below at a temperature of 121 °C. 15 samples were tested with resin and five samples were tested without.

Table 5.2 Peak forming force comparison between SBCF samples with and without resin impregnation

Single Tow Forming Test

Plunger diameter: 19.05 mm Gap width: 53.98 mm

	Standard Deviation	Average Peak Force (N)
With Resin	0.41	1.31
Without Resin	0.12	3.51

The results from Table 5.2 indicate that the resin held slightly less peak force results towards samples without resin as expected. At elevated temperatures, the resin's viscosity becomes lowered and allows less friction between the fibers and the matrix. To further illustrate this point, another round of tests was performed where a large bead of resin was placed in between the tool and the ply. This is illustrated below in Figure 5.11.

Figure 5.11: Extra resin placed between the tool and the ply

Upon conducting tests with a constant plunger size of 19.05 mm and gap widths of 28.58 mm and 53.98 mm, it was evident that there existed a significant variation in the peak forming force at elevated temperature (refer to Figure 5.12).

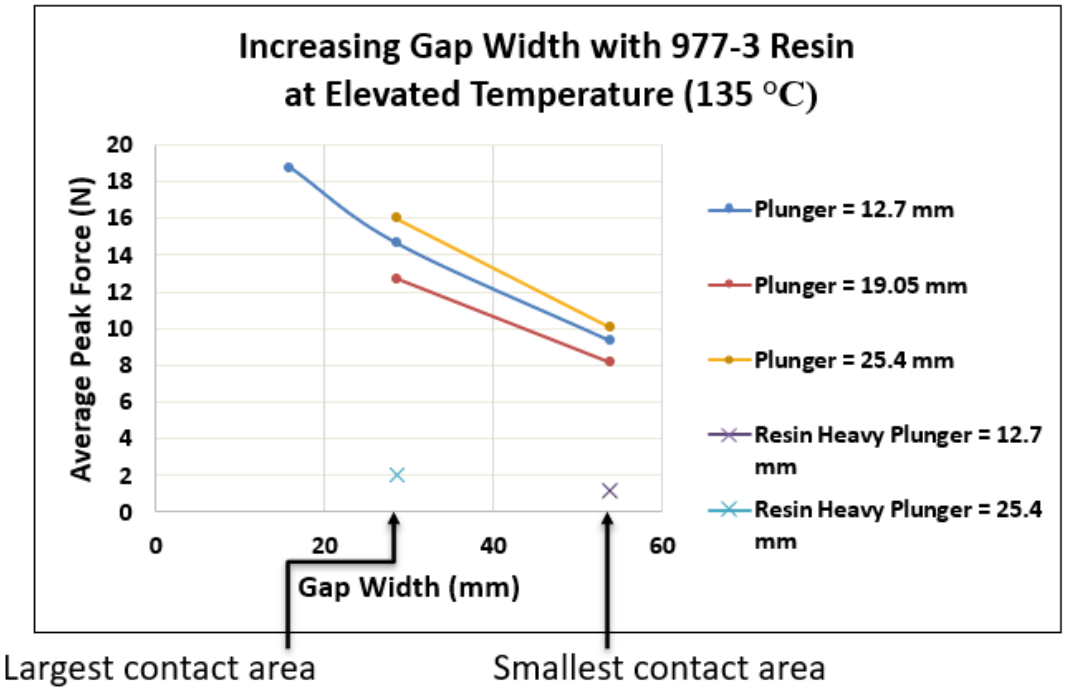

Figure 5.12: Vast difference in peak force with extra resin placed between the tool and ply

Conclusions

This research investigated forming capabilities of resin impregnated stretch broken carbon fiber. The importance of this work was to understand how well the SBCF would form in the forming cycle as well as come up with data that provided insight as to where the most resistance took place. This was done by subjecting the materials to differential geometric loading parameters from a novel forming fixture and quantifying them by collecting the load versus displacement data.

The first objective investigated the effect of increasing gap length, which simulated the width of a 90°C-channel and how forming loads would be affected by the increasing gap between the vertical segments. It was determined that the width of the gap displayed a decrease in yield force required for stretching. These values were between 38 and 16 N for 8552 and 18 and 7 N for 977-3 at elevated temperatures.

The second objective prioritized the augmentation of the plunger's dimensions. This aspect held significant importance, as it aimed to replicate the applied force exerted between the ply and the vacuum bag, thereby ensuring a snug fit within the mold, particularly as the contact area expanded. Based on the data analysis, it was observed that modifying these parameters yielded negligible variations in the peak forming loads. Specifically, the disparities in peak forces amounted to 5 N for 8552 and 3 N for 977-3.

The third objective was to compare objectives one and two to data accumulated at room temperature. The importance was to provide insight on how elevated temperatures were required to achieve a low forming force (100 times less), and that there would be no unwanted stretching of the fibers due to the handling of the material during the layup process.

The fourth objective investigated the effect of resin quantities between the tool and ply with respect to peak load. It was determined that SBCF tows with resin shared slightly less peak force (~37%) from tows with only sizing application. In addition, including an arbitrary lubrication layer of resin between the tool and ply contributed the smallest amount of peak force (1-2 N).

CHAPTER SIX

CONCLUSIONS AND FUTURE WORK

Results of research based on thesis objectives

1. *Continuation to conduct gauge length study of CF tows to understand differences in continuous and stretch broken tensile behavior.*

This study compared the tensile properties of short-bead carbon fibers (SBCF) with continuous carbon fiber tows under varying gauge lengths and temperatures. The experimental data revealed that the tensile strength of both SBCF and continuous fibers decreased with increasing gauge length due to the increased number of inherent flaws in the material. Furthermore, elevated temperature resulted in a loss of sizing functionality, contributing to a reduction in peak forces. Notably, the MSU SBCF with a mean fiber length of 30 mm exhibited substantially lower peak forces than the Hexcel SBCF with a mean fiber length of 50.8 mm [2]. SBCF and Hexcel SBCF showed almost 10 times lower peak forces than continuous carbon fiber tows. As the gauge length exceeded the mean fiber length of SBCF, the stresses approached 0 MPa. The study demonstrated the potential of SBCF for lowering the manufacturability time by allowing the formation of entire layups under vacuum pressure alone, which could ultimately save time and resources.

2. *Tensile properties of stretch broken carbon fiber prepreg.*

A custom thermal enclosure was designed to provide uniform heating for a prepreg tow of stretch broken carbon fiber (SBCF) to investigate true stress versus true strain. This study characterized the true stress and true strain of single tow SBCF prepreg at elevated temperatures of 121 +/-5 ºC for 8552 resin and 135 +/-5 ºC for 977-3 resins. The test was conducted following

a one-dimensional tensile test at a constant displacement rate of 6.3 mm/min. The experimental analysis showed that the material exhibited strain softening behavior when subjected to 8552 and 977-3 epoxy resin systems. This was confirmed through the presence of shear planes in the tensile test samples. The observed strain softening behavior was unaffected by the shear forces between plies as more plies were added to the test sample at different fiber orientations.

3. *Forming properties of stretch broken carbon fiber prepreg on a novel forming fixture.*

After many iterations of the forming fixture was designed to accurately test CFRP ribbons and tows, data was collected in the stretch-bending condition. This research investigated forming capabilities of resin impregnated stretch broken carbon fiber. This work was essential to understand how the SBCF will form in the forming cycle. This was done by subjecting the materials to differential geometric loading parameters and quantifying them by collecting the load versus displacement data. It was determined that as the gap between the heated blocks increases, the peak force decreases for both 8552 and 977-3 resin systems at both elevated and room temperatures (20 °C – 135 °C). Due to the differences in the mechanical and rheological properties of the two resins, 8552 resin had twice the peak force (18 N versus 39 N) to that of the 977-3 resin at the most complex geometries. Peak forces between the two resin types had minimal differences in peak force when tested at room temperature. It was also determined that SBCF tows with resin shared slightly less peak force (~37%) from tows with only sizing application.

Recommendations for future work

1. *Continuation to conduct gauge length study of CF tows to understand differences in continuous and stretch broken tensile behavior.*

While this experiment tested samples at a constant rate, one may introduce different load rates to investigate the rate dependence on peak tensile loads. The elevated temperature was 100 °C. One may introduce higher temperatures since the typical debulking temperatures are much higher in real applications.

2. Tensile properties of stretch broken carbon fiber prepreg.

With this fundamental data being recorded at the prepreg's tow level, future work would require investigating this behavior with larger and thicker samples under more relatable environmental conditions. Better areal measurements could be recorded with real time digital micrometers along the gauge length of the test specimen. It would be most desirable to continue testing the material as it evolves in improved manufacturing process.

3. Forming properties of stretch broken carbon fiber prepreg on a novel forming fixture.

As the forming fixture used in this experiment resulted in many iterative designs and ideas, it would be recommended to manufacture another with a more geometrical range. In that, one that can test wider gaps and different geometric profiles. Continuing work was being done to investigate peak forming loads with respect to different resin viscosities being controlled by different elevated tool temperatures and rate dependence. Investigating samples with different ply thicknesses and multiaxial orientations would also be recommended to relate ply friction concerning peak force. Overall, this data could be validated using FEA which would lead to simulating load parameters utilized in the design of the forming process.

REFERENCES CITED

[1] C. Soutis "Carbon fiber reinforced plastics in aircraft construction," Mat Sci and Eng 2005 https://doi.org/10.1016/j.msea.2005.08.064.

[2] J. Janicki et al. "Gauge length and temperature influence on the tensile properties of stretch broken carbon fiber tows." Composites Part A: Applied Science and Manufacturing https://doi.org/10.1016/j.compositesa.2021.106426

[3] Where the Road Forks, "Titanium vs carbon fiber bike: pros and cons," Bikes and Cycling 2022 https://wheretheroadforks.com/titanium-vs-carbon-fiber-bike-pros-and-cons

[4] G. Jacobsen Mechanical characterization of stretch broken carbon fiber materials," In Proceedings of SAMPE'09 Spring Symposium Technical Conference 2007

[5] J. Günther, "Characterization of stretch broken fiber composites – IM7 fiber 8552 resin – stretch at prepreg level," In: Proceedings of SAMPE 2011, Long Beach, CA, 2011

[6] J. Günther, "Process Development and Characterization of Stretch Broken Carbon Fiber Materials," In Proceedings of SAMPE'09 Spring Symposium Technical Conference. Memphis, TN, 2007

[7] WorldAutoSteel, "Engineering Stress-Strain vs. True Stress-Strain 2020," https://ahssinsights.org/forming/formability/engineering-stress-strain-true-stress-strain/

[8] M. Egloff et al. "A Predictive Forming Model for Stretch-Broken Carbon Fiber Composites as a Function of State of Stress, Forming Rate, and Resin Viscosity," In proceedings of CAMX Anaheim CA, October 2022

[9] Y. Shchemelinin et al.: Bulge and dome testing to investigate the formability of continuous and stretch broken carbon fiber prepreg laminates. In proceedings of CAMX Anaheim CA, October 2022

[10] R. Morshed Rezaul et al. "Effect of process variables on the uncured handleability and formability of stretch broken carbon fiber," In proceedings of CAMX Anaheim CA, October 2022

[11] T. Javin Nur et al. "Novel experimental unit to evaluate inter-ply and tool-ply friction in carbon fiber reinforced polymer composites prepregs," In proceedings of CAMX Anaheim CA, October 2022

[12] C. Ridgard, D. Cairns, "Advances in the development of stretch broken carbon fiber for primary aircraft structure," In proceedings of CAMX Anaheim CA, October 2022

[13] D. Nold et al. "Tensile properties of stretch broken carbon fiber prepreg," In proceedings of CAMX Anaheim CA, October 2022

[14] J. C. Janicki, M. C. Egloff et al. "Formability characterization of fiber reinforced polymer composites using a novel test method," Journal of Testing and Evaluation, October 2021 https://doi.org/10.1520/JTE20210250

[15] R. M. Rezaul "Effect of process variables on the uncured handleability and formability of stretch broken carbon fiber," Master's thesis from Montana State University Dec 2022

[16] N.M. Loomis "Preliminary mechanical testing of continuous stretch broken carbon fiber cured laminates", Master's thesis from Montana State University May 2022

[17] Abureden, Ghaith A., Walid M. Hasan, and Ayman N. Ababneh. "Exploring potential benefits of additive manufacturing in creating corrugated web steel beams." Journal of Constructional Steel Research 187 (2021): 106975.

[18] J. Cao and L. Chen, "Effect of thermal cycling on carbon fiber-reinforced PPS composites," in SEM Annual Conference and Exposition on Experimental & Applied Mechanics, Portland, 2005.

[19] A. (2022, November 22). Vacuum Forming Process. DitaiPlastic. https://www.ditaiplastic.com/vacuum-forming-process/

[20] Hexcel Corporation, HexTow IM7 Carbon Fiber Product Data Sheet, Stamford, CT, 2020.

[21] J. Janicki "Forming parameters and quantifications of continuous and stretch broken carbon fibers", Master's thesis from Montana State University Dec 2021

[22] Deletombe, Eric, et al. "Improvement of numerical methods for crash analysis in future composite aircraft design." *Aerospace science and technology* 4.3 (2000): 189-199. https://doi.org/10.1016/S1270-9638(00)00126-7

[23] Kalanchiam, Muniyasamy, and Moorthy Chinnasamy. "Advantages of composite materials in aircraft structures." *International Journal of Aerospace and Mechanical Engineering* 6.11 (2012)

[24] Peters, S T, Humphrey, W D, Foral, R F, Westinghouse Electric Corp., Marine Div., Sunnyvale, CA, and Brunswick Corp., Defense Div., Lincoln, NE). Filament winding - Composite structure fabrication. United States: N. p., 1991. Web.

[25] Calado, Elcin Aleixo, Marco Leite, and Arlindo Silva. "Selecting composite materials considering cost and environmental impact in the early phases of aircraft structure design." *Journal of Cleaner Production* 186 (2018): 113-122. https://doi.org/10.1016/j.jclepro.2018.02.048

[26] Joseph, Blessy, et al. "Cellulose nanocomposites: Fabrication and biomedical applications." *Journal of Bioresources and Bioproducts* 5.4 (2020): 223-237. https://doi.org/10.1016/j.jobab.2020.10.001

[27] Martin, Lockheed. "F-22 RAPTOR: Air dominance for the 21st century." *Advanced materials & processes* 153.5 (1998): 23.

[28] Greaves, George Neville, et al. "Poisson's ratio and modern materials." *Nature materials* 10.11 (2011): 823-837.

[29] Arasaratnam, P., K. S. Sivakumaran, and M. J. Tait. "True stress-true strain models for structural steel elements." *International Scholarly Research Notices* 2011 (2011).

APPENDIX

Method

Null hypothesis	All means are equal
Alternative hypothesis	Not all means are equal
Significance level	α = 0.05

Equal variances were assumed for the analysis.

A.1: Statistical method

Means

Factor	N	Mean	StDev	95% CI
0.25" Gauge Length_Max Stress	5	3350.3	92.3	(3128.9, 3571.7)
0.5" Gauge Length_Max Stress	5	2999	452	(2778, 3221)
1.0" Gauge Length_Max Stress	5	2992.5	153.6	(2771.1, 3213.9)
2.0" Gauge Length_Max Stress	5	2848	230	(2627, 3070)
3.0" Gauge Length_Max Stress	5	2678.4	195.1	(2457.0, 2899.8)
4.0" Gauge Length_Max Stress	5	2622.5	216.3	(2401.1, 2844.0)
5.0" Gauge Length_Max Stress	5	2796.2	186.0	(2574.8, 3017.7)

Pooled StDev = 241.686

Analysis of Variance

Source	DF	Adj SS	Adj MS	F-Value	P-Value
Factor	6	1803631	300605	5.15	0.001
Error	28	1635543	58412		
Total	34	3439174			

A.2: Continuous ambient temperature max stress ANOVA

Means

Factor	N	Mean	StDev	95% CI
0.25" Gauge Length_Max Stress	5	3067.8	124.7	(2931.8, 3203.7)
0.5" Gauge Length_Max Stress	5	3048.5	102.7	(2912.5, 3184.5)
1.0" Gauge Length_Max Stress	5	2881.8	191.7	(2745.8, 3017.7)
2.0" Gauge Length_Max Stress	5	2466.2	152.1	(2330.2, 2602.2)
3.0" Gauge Length_Max Stress	5	2225.8	135.8	(2089.8, 2361.8)
4.0" Gauge Length_Max Stress	5	2223.4	124.8	(2087.4, 2359.4)
5.0" Gauge Length_Max Stress	5	1947.3	185.0	(1811.3, 2083.3)

Pooled StDev = 148.441

Analysis of Variance

Source	DF	Adj SS	Adj MS	F-Value	P-Value
Factor	6	6043506	1007251	45.71	0.000
Error	28	616976	22035		
Total	34	6660482			

A.3: Continuous elevated temperature max stress ANOVA

Means

Factor	N	Mean	StDev	95% CI
0.25" Gauge Length_Max Stress	5	1943	264	(1790, 2096)
0.5" Gauge Length_Max Stress	5	1609.5	180.3	(1456.6, 1762.4)
1.0" Gauge Length_Max Stress	5	1527.5	150.8	(1374.6, 1680.4)
2.0" Gauge Length_Max Stress	5	1240	225	(1087, 1393)
3.0" Gauge Length_Max Stress	5	1349.2	79.9	(1196.3, 1502.1)
4.0" Gauge Length_Max Stress	5	1475.3	104.2	(1322.4, 1628.2)
5.0" Gauge Length_Max Stress	5	1538.2	45.8	(1385.3, 1691.1)

Pooled StDev = 166.903

Analysis of Variance

Source	DF	Adj SS	Adj MS	F-Value	P-Value
Factor	6	1483524	247254	8.88	0.000
Error	28	779984	27857		
Total	34	2263507			

A.4: MSU SBCF ambient temperature max stress ANOVA

Means

Factor	N	Mean	StDev	95% CI
0.25" Gauge Length_Max Stress	5	1616	291	(1502, 1731)
0.5" Gauge Length_Max Stress	5	1049.2	137.7	(934.9, 1163.5)
1.0" Gauge Length_Max Stress	5	248.1	71.0	(133.8, 362.4)
2.0" Gauge Length_Max Stress	5	42.75	3.47	(-71.54, 157.05)
3.0" Gauge Length_Max Stress	5	42.75	4.08	(-71.54, 157.05)
4.0" Gauge Length_Max Stress	5	35.63	3.41	(-78.67, 149.92)
5.0" Gauge Length_Max Stress	5	39.95	4.89	(-74.35, 154.24)

Pooled StDev = 124.767

Analysis of Variance

Source	DF	Adj SS	Adj MS	F-Value	P-Value
Factor	6	12156120	2026020	130.15	0.000
Error	28	435871	15567		
Total	34	12591991			

A.5: MSU SBCF elevated temperature max stress ANOVA

Means

Factor	N	Mean	StDev	95% CI
Disp. 0.46 mm	5	5.534	0.724	(5.159, 5.909)
Disp. 1 mm	5	4.220	0.259	(3.845, 4.595)
Disp. 2 mm	5	3.165	0.434	(2.791, 3.540)
Disp. 3 mm	5	2.783	0.382	(2.408, 3.158)
Disp. 4 mm	5	1.597	0.393	(1.223, 1.972)
Disp. 5 mm	5	2.0166	0.1212	(1.6418, 2.3914)
Disp. 6 mm	5	1.621	0.278	(1.246, 1.995)

Pooled StDev = 0.409142

Analysis of Variance

Source	DF	Adj SS	Adj MS	F-Value	P-Value
Factor	6	64.102	10.6837	63.82	0.000
Error	28	4.687	0.1674		
Total	34	68.790			

A.6: 977-3 True stress ANOVA

Means

Factor	N	Mean	StDev	95% CI
Disp. 0.39 mm	5	4.337	0.704	(3.746, 4.928)
Disp. 1 mm	5	3.734	0.450	(3.143, 4.326)
Disp. 2 mm	5	3.567	0.872	(2.976, 4.159)
Disp. 3 mm	5	2.497	0.377	(1.906, 3.088)
Disp. 4 mm	5	2.444	0.889	(1.853, 3.035)
Disp. 5 mm	5	1.802	0.516	(1.211, 2.394)
Disp. 6 mm	5	2.008	0.508	(1.417, 2.600)

Pooled StDev = 0.645396

Analysis of Variance

Source	DF	Adj SS	Adj MS	F-Value	P-Value
Factor	6	27.87	4.6457	11.15	0.000
Error	28	11.66	0.4165		
Total	34	39.54			

A.7: 8552 True stress ANOVA

Means

Factor	N	Mean	StDev	95% CI
Gap: 15.8 mm	4	17.77	2.13	(16.26, 19.27)
Gap: 28.58 mm	5	14.388	0.907	(13.040, 15.736)
Gap: 53.98 mm	5	9.332	0.958	(7.984, 10.680)

Pooled StDev = 1.36908

Analysis of Variance

Source	DF	Adj SS	Adj MS	F-Value	P-Value
Factor	2	163.53	81.767	43.62	0.000
Error	11	20.62	1.874		
Total	13	184.15			

A.8: 977-3 increasing gap length at elevated temperature with plunger diameter of 12.7 mm ANOVA

Means

Factor	N	Mean	StDev	95% CI
Plunger: 12.7 mm	5	14.388	0.907	(13.112, 15.664)
Plunger: 19.05 mm	4	13.320	1.379	(11.893, 14.747)
Plunger: 25.4 mm	5	15.992	1.541	(14.716, 17.268)

Pooled StDev = 1.29674

Analysis of Variance

Source	DF	Adj SS	Adj MS	F-Value	P-Value
Factor	2	16.42	8.212	4.88	0.030
Error	11	18.50	1.682		
Total	13	34.92			

A.9: 977-3 increasing plunger diameter at elevated temperature with a gap size of 28.58 mm ANOVA

Means

Factor	N	Mean	StDev	95% CI
Gap: 15.88 mm	4	38.90	4.57	(35.22, 42.58)
Gap: 28.58 mm	5	20.72	3.21	(17.43, 24.01)
Gap: 53.98 mm	5	18.468	2.181	(15.181, 21.755)

Pooled StDev = 3.33988

Analysis of Variance

Source	DF	Adj SS	Adj MS	F-Value	P-Value
Factor	2	1077.6	538.80	48.30	0.000
Error	11	122.7	11.15		
Total	13	1200.3			

A.10: 8552 increasing gap size at elevated temperature with a plunger diameter of 28.58 mm ANOVA

Means

Factor	N	Mean	StDev	95% CI
Plunger: 12.7 mm	5	20.72	3.21	(18.09, 23.35)
Plunger: 19.05 mm	5	22.12	2.48	(19.49, 24.75)
Plunger: 25.4 mm	5	24.20	2.32	(21.57, 26.83)

Pooled StDev = 2.69874

Analysis of Variance

Source	DF	Adj SS	Adj MS	F-Value	P-Value
Factor	2	30.58	15.288	2.10	0.165
Error	12	87.40	7.283		
Total	14	117.98			

A.11: 977-3 increasing plunger diameter at elevated temperature with a gap size of 28.58 mm ANOVA